

A New Two-Dimensional Blood Flow Model and Its RKDG Approximation

Yolhan Mannes¹, Mehmet Ersoy¹, Ömer Faruk Eker², Aimed Ajroud³

¹Institut de Mathématiques de Toulon (IMATH), Université de Toulon, La Garde, France

²CHU de Bordeaux, Université Claude Bernard Lyon 1, Bordeaux and Lyon, France

³Ecole d'ingénieurs Seatech, Université de Toulon, Toulon, France

Email: yolhan@laposte.net, ersoy@univ-tln.fr, pousselcamille@outlook.fr, aimed.ajroud@univ-tln.fr

How to cite this paper: Mannes, Y., Ersoy, M., Eker, Ö.F. and Ajroud, A. (2025) A New Two-Dimensional Blood Flow Model and Its RKDG Approximation. *Journal of Applied Mathematics and Physics*, **13**, 3930-3967. <https://doi.org/10.4236/jamp.2025.1311220>

Received: September 26, 2025

Accepted: November 15, 2025

Published: November 18, 2025

Copyright © 2025 by author(s) and Scientific Research Publishing Inc.

This work is licensed under the Creative Commons Attribution International License (CC BY 4.0).

<http://creativecommons.org/licenses/by/4.0/>



Open Access

Abstract

We propose a new two-dimensional blood flow reduced model taking into account of complex artery geometry as in the case of severe aneurysm. We derive the model from the three-dimensional Navier-Stokes equations written in a curvilinear coordinate system under the thin-artery assumption, with boundary conditions including wall tissue deformation. We show that the model is energetically consistent with the full Navier-Stokes problem. This model, obtained via radial averaging, is, up to our knowledge, the first one. It has the advantage of being more accurate than the classical one-dimensional models and being solved in a reasonable time in comparison with the Navier-Stokes models. To this purpose, we use a Runge-Kutta Discontinuous Galerkin (RKDG) method to solve the two-dimensional problem. We end the paper with several numerical test cases to show the efficiency and robustness of the numerical model, and in particular, we show the limit of the one-dimensional models in the case of a severe aneurysm.

Keywords

Blood Flow, Asymptotic Analysis, Thin-Artery Assumption, Energy Consistency, RKDG Method, Aneurysm

1. Introduction

Modeling the cardiovascular system in arteries holds a central place in medical science, particularly in connection with cardiovascular diseases such as coronary heart disease, stroke, peripheral artery disease, aneurysms, and others. This is especially important today in understanding and forecasting the impact of developed countries' way of life on people's healthcare (around 30% of cardiovascular

disease deaths are from developed countries). Therefore, it is of major interest to develop an accurate mathematical model.

The dynamic of such flow is mainly influenced by the fluid-structure interaction with the artery wall. The forecast to predict the motion of blood through the artery is a difficult task to which substantial effort has been devoted [1]-[8].

One of the most widely used models to describe the motion of blood through the artery is the one-dimensional (1D) Blood Flow equation derived, for instance, in [1] [5] [6] [9]-[11]. This classical model is a hyperbolic system of Partial Differential Equations (PDE) describing the conservation laws linking the wall elasticity to the fluid dynamics. This model is derived from an ansatz for the velocity profile in Equation (2) and reads,

$$\begin{cases} \partial_t A + \partial_x Q = 0, \\ \partial_t Q + \partial_x \left(\alpha \frac{Q^2}{A} + \frac{1}{\rho} AP(A, x) \right) = \frac{1}{\rho} P(A, x) \partial_x A - K \frac{Q}{A}, \end{cases} \quad (1)$$

where the unknowns $A(t, x)$ stands artery's section area (assumed to be cylindrical), $Q(t, x) = A(t, x) \bar{u}_x(t, x)$ is the flow rate and \bar{u}_x is the mean speed over the artery's section (see [1] [6] for further details). The function $P(A, x)$ denotes the pressure of blood at the wall and reads,

$$P(A, x) = b(x) \frac{\sqrt{A} - \sqrt{A_0}}{A_0},$$

where b encompasses the elastic behavior of the artery, *i.e.*, $b(x) = \frac{E(x)}{1-\xi} h \sqrt{\pi}$, where E is the Young's modulus, ξ is the Poisson ratio, and h is the wall thickness. The velocity profile is given by

$$u_x(t, r, x) = \frac{Q(t, x)}{A(t, x)} \frac{\gamma + 2}{\gamma} \left[1 - \left(\frac{r}{R(t, x)} \right)^\gamma \right], \quad (2)$$

where γ is an integer (often set to 9, see for instance [6] [12]). The friction term K is defined as a function of γ by $K = 2\pi\nu(\gamma + 2)$ where ν is the kinematic viscosity of the blood. In Equation (1), the Bousinesq coefficient is given by $\alpha = \frac{\gamma + 2}{\gamma + 1}$ (*c.f.* [6] [7] [12]). In recent work, inspired from [13]-[15], an inviscid hyperbolic one-dimensional model and a viscous one was derived without the ansatz assumption and by section-averaging techniques. These models are

$$\begin{cases} \partial_t A + \partial_x Q = 0, \\ \partial_t Q + \partial_x \left(\frac{Q^2}{A} + \frac{1}{\rho} AP(A, x) \right) = \frac{1}{\rho} P(A, x) \partial_x A + 2\pi Rk \frac{Q}{A}, \end{cases} \quad (3)$$

$$\begin{cases} \partial_t A + \partial_x Q = 0, \\ \partial_t Q + \partial_x \left(\frac{Q^2}{A} + \frac{1}{\rho} AP(A, x) \right) - \partial_x \left(3\nu A \partial_x \left(\frac{Q}{A} \right) \right) = \frac{1}{\rho} P(A, x) \partial_x A + \frac{2\pi Rk}{1 - \frac{Rk}{4\nu}} \frac{Q}{A}, \end{cases} \quad (4)$$

where $R(t, x)$ is the radius, $A = \pi R^2$ the area, $Q = \overline{Au_x}$ the flow rate, $\overline{u_x}$ the mean speed of blood per section, ρ the density of blood, P , the pressure, ν the kinematic viscosity, and k a negative friction coefficient. For these models, several mathematical and physical properties have been obtained. These two new one-dimensional models, while similar to existing ones in the literature, are derived using a well-known technique used, for instance, in [14]-[16]. This method allows the construction of each asymptotic term one by one, distinguishing it from the classical approach using ansatz (see Equation (1) and [6]). The most notable advantage of these one-dimensional models is the ease of implementation of fast and robust numerical methods and providing good results in the context of quasi-cylindrical arteries.

Although, in the presence of aneurysms, both previously derived models may suffer from precision issues due to the non-uniform deformation in the radial direction [17]. To avoid those issues a three-dimensional model can be used, however, it leads to costly numerical computations. This leads to our idea of developing the first two-dimensional blood flow model in complex artery geometry. This new model reads

$$\begin{cases} \partial_t A + \partial_\theta \left(\frac{Q_{R\theta}}{A} \right) + \partial_s (Q_s) = 0, \\ \partial_t (Q_{R\theta}) + \partial_\theta \left(\frac{Q_{R\theta}^2}{2A^2} + AP \right) + \partial_s \left(\frac{Q_{R\theta} Q_s}{A} \right) = \frac{2R}{3} C \sin \theta \frac{Q_s^2}{A} + 2Rk \frac{Q_{R\theta}}{A} + \partial_\theta AP, \\ \partial_t (Q_s) + \partial_\theta \left(\frac{Q_s Q_{R\theta}}{A^2} \right) + \partial_s \left(\frac{Q_s^2}{A} - \frac{Q_{R\theta}^2}{2A^2} + AP \right) = -\frac{2R}{3} C \sin \theta \frac{Q_s Q_{R\theta}}{A^2} + kR \frac{Q_s}{A} + \partial_s AP, \\ P = P_{ext} + b \frac{R - R_0}{R_0^2}. \end{cases} \tag{5}$$

where $A(t, \theta, s)$ is now define as $\frac{R^2}{2}$ with s the curvilinear abscissa and θ the angle, $Q_{R\theta} = \frac{3}{4} RA \overline{u_\theta}$, $Q_s = \overline{Au_s}$, P the pressure, C the curvature of the artery and k a negative friction coefficient. This new model takes into account the variations of the geometry more accurately than one-dimensional models and yields to less expensive numerical method than the three-dimensional ones.

We outline the rest of the paper as follows: in Section 2, as our starting point we present the Navier-Stokes equations and the boundary conditions including friction and the wall law deformation. We derive the radial-averaged two-dimensional equations. In Section 3, we use a Discontinues Galerkin (DG) method from [18] called the Runge-Kutta Discontinues Galerkin method (RKDG). We use explicit Runge-Kutta for time integration. We provide extensive numerical testing in Section 4 of the resulting code. A Julia¹ implementation of this code, written by Y. Mannes and M. Ersoy, is freely available on request.

¹<https://julialang.org/>.

2. On the Derivation of a New Two-Dimensional Model for Blood Flow in Arteries

In this section, we present the full derivation of the new two-dimensional model for blood flow (Equation (5)) starting from the Navier-Stokes equations.

2.1. Navier-Stokes Equations in a Curvilinear Coordinate System

We aim to construct a mathematical model for blood flow in an artery consistent with the phenomena that can affect its motion. We propose a model reduction of the three-dimensional Navier-Stokes equations leading to a new two-dimensional model following the technique in [14]-[16]. We study the case of a curvilinear artery (with a star-like cross-section, see **Figure 1**) and consider suitable boundary conditions to account for artery wall radial deformation and friction. In contrast with existing models for which the radius is θ -independent, we assume here that the radius is a function of θ , thus yielding radial non-uniform deformation. This assumption allows us to, accurately, describe aneurysms, stenosis, etc.

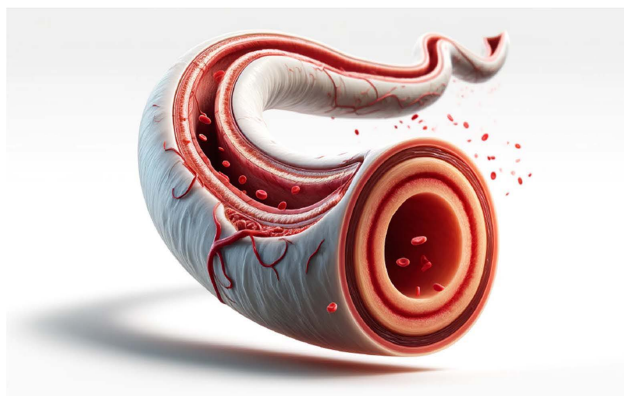


Figure 1. Artery shape.

We start in Subsection 2.1.1 by reviewing the Navier-Stokes equations in a curvilinear coordinate frame (using a Serret-Frenet in a cylindrical framework), describing the physics with the artery wall boundary. We then introduce the boundary condition at the wall in Subsection 2.1.2.

2.1.1. Geometric Set-Up and the Three-Dimensional Navier-Stokes Equations in Curvilinear Coordinates

Regarding arteryshape2d, we consider arteries with star-like cross-sections, meaning, all cross-sections are convex to a curve $c \in C^3([0, L], \mathbb{R}^3)$ with L the length of the artery, and belong to the orthogonal plane to $c'(s)$, where s stands for the curvilinear abscissa. Moreover, we suppose c verifies $\|c'(s)\|_{\mathbb{R}^3} = 1$ for all $s \in [0, L]$ and $\|c''(s)\|_{\mathbb{R}^3} \neq 0$ for all $s \in [0, L]$.

We consider an incompressible fluid moving in the time-space domain

$$\Omega = \left\{ (x, y, z) \in \mathbb{R}^3; \|(x, y, z) - c(s(x, y, z))\|_{\mathbb{R}^3} \leq R(t, x, y, z), s(x, y, z) \in [0, L], t \in [0, T] \right\}, \quad (6)$$

where, $s(x, y, z)$ is such that (x, y, z) belongs to the orthogonal plane of $c'(s)$ as displayed in **Figure 2**, $R(t, x, y, z)$ is the radius of the cross-section at a particular angle θ and $T > 0$ an arbitrary final time.

We assume that the velocity \mathbf{u} of the viscous flow satisfies, on the domain Ω , the three-dimensional incompressible Navier-Stokes equations

$$\begin{cases} \operatorname{div} \mathbf{u} = 0, \\ \partial_t \mathbf{u} + \operatorname{div}(\mathbf{u} \otimes \mathbf{u}) + \nabla p - \operatorname{div} \sigma = 0, \end{cases} \quad (7)$$

where $\mathbf{u} = u_x \mathbf{i} + u_y \mathbf{j} + u_z \mathbf{k}$ with $(\mathbf{i}, \mathbf{j}, \mathbf{k})$ the cartesian basis, $p = \frac{P}{\rho}$ where P is the pressure and ρ , the density of the fluid. Finally, the stress tensor is $\sigma = \nu(\nabla \mathbf{u} + (\nabla \mathbf{u})^t)$ where ν is the kinematic viscosity. Consider the following change of variable,

$$\mathbf{e}_r(\theta, s) = \cos \theta \mathbf{n}(s) + \sin \theta \mathbf{b}(s), \quad \mathbf{e}_\theta(\theta, s) = -\sin \theta \mathbf{n}(s) + \cos \theta \mathbf{b}(s), \quad (8)$$

where $\mathbf{t}(s) = c'(s)$, $\mathbf{n}(s) = \frac{c''(s)}{\mathcal{C}(s)}$, and $\bar{\mathbf{b}}(s) = \bar{\mathbf{t}}(s) \wedge \bar{\mathbf{n}}(s)$ with

$\mathcal{C}(s) = \|c''(s)\|_{\mathbb{R}^3}$ for all $s \in [0, L]$, the curvature of the artery, then the domain Ω from Equation (6) is expressed as

$$\Omega = \{c(s) + r\mathbf{e}_r(\theta, s) \in \mathbb{R}^3 \mid r \in [0, R(t, x)], \theta \in [0, 2\pi], s \in [0, L], t \in [0, T]\}.$$

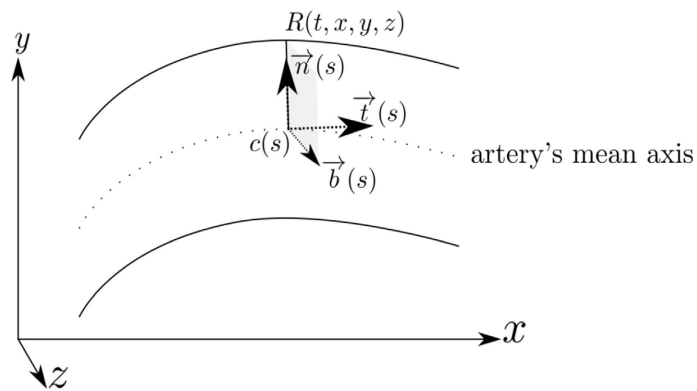


Figure 2. Serret frenet frame.

The velocity $\mathbf{u} = u_r \mathbf{e}_r + u_\theta \mathbf{e}_\theta + u_s \mathbf{t}$ where u_r is the radial speed, u_θ is the angular speed and u_s is the axial speed.

The coordinate transformation reads $M(r, \theta, s) = c(s) + r\mathbf{e}_r(\theta, s)$ leading to

the following Jacobian matrix, $A^{-1} = \begin{pmatrix} 1 & 0 & 0 \\ 0 & r & r\mathcal{T} \\ 0 & 0 & \beta \end{pmatrix}_{\mathbf{e}_r, \mathbf{e}_\theta, \mathbf{t}}$ where

$$\mathcal{T}(s) = \frac{1}{\mathcal{C}^2(s)} \det(c'(s), c''(s), c^{(3)}(s))$$

is the torsion of the curve and

$$\beta(r, \theta, s) = 1 - r\mathcal{C}(s) \cos \theta.$$

The inverse Jacobian matrix then reads,

$$A = \frac{1}{J} \begin{pmatrix} r\beta & 0 & 0 \\ 0 & \beta & -rT \\ 0 & 0 & r \end{pmatrix}_{e_r, e_\theta, t} \quad \text{where } J = r\beta = \det(A^{-1}). \text{ Coordinate change in}$$

$$\text{Equation (8) leads to } \nabla p = \begin{pmatrix} \partial_r p \\ \frac{1}{r} \partial_\theta p \\ \frac{\partial_s p - T(s) \partial_\theta p}{\beta} \end{pmatrix}_{e_r, e_\theta, t} = \begin{pmatrix} \partial_r p \\ \frac{1}{r} \partial_\theta p \\ \frac{\partial_T p}{\beta} \end{pmatrix}_{e_r, e_\theta, t} \quad \text{where}$$

$$\partial_T = \partial_s - T \partial_\theta, \text{ and,}$$

$$\text{div } \mathbf{u} = \frac{1}{r\beta} \partial_r (r\beta u_r) + \frac{1}{r\beta} \partial_\theta (\beta u_\theta) + \frac{1}{r\beta} \partial_T (ru_s),$$

$$\nabla \mathbf{u} = \begin{pmatrix} \partial_r u_r & \partial_r u_\theta & \partial_r u_s \\ \frac{\partial_\theta u_r - u_\theta}{r} & \frac{\partial_\theta u_\theta + u_r}{r} & \frac{\partial_\theta u_s}{r} \\ \frac{\partial_T u_r + C \cos \theta u_s}{\beta} & \frac{\partial_T u_\theta - C \sin \theta u_s}{\beta} & \frac{\partial_T u_s - C (\cos \theta u_r - \sin \theta u_\theta)}{\beta} \end{pmatrix}_{e_r, e_\theta, t},$$

$$\text{div } \sigma = \begin{pmatrix} \frac{1}{r\beta} \partial_r (r\beta \sigma_{rr}) + \frac{1}{r\beta} \partial_\theta (\beta \sigma_{\theta r}) + \frac{1}{r\beta} \partial_T (r\sigma_{sr}) - \frac{1}{r} \sigma_{\theta\theta} + \frac{C \cos \theta}{\beta} \sigma_{ss} \\ \frac{1}{r\beta} \partial_r (r\beta \sigma_{r\theta}) + \frac{1}{r\beta} \partial_\theta (\beta \sigma_{\theta\theta}) + \frac{1}{r\beta} \partial_T (r\sigma_{s\theta}) + \frac{1}{r} \sigma_{\theta r} - \frac{C \sin \theta}{\beta} \sigma_{ss} \\ \frac{1}{r\beta} \partial_r (r\beta \sigma_{rs}) + \frac{1}{r\beta} \partial_\theta (\beta \sigma_{\theta s}) + \frac{1}{r\beta} \partial_T (r\sigma_{ss}) - \frac{C}{\beta} (\cos \theta \sigma_{sr} - \sin \theta \sigma_{s\theta}) \end{pmatrix}_{e_r, e_\theta, t},$$

where,

$$\sigma = \begin{pmatrix} \sigma_{rr} & \sigma_{r\theta} & \sigma_{rs} \\ \sigma_{\theta r} & \sigma_{\theta\theta} & \sigma_{\theta s} \\ \sigma_{sr} & \sigma_{s\theta} & \sigma_{ss} \end{pmatrix}_{e_r, e_\theta, t}$$

$$= \nu \begin{pmatrix} 2\partial_r u_r & \partial_r u_\theta + \frac{\partial_\theta u_r - u_\theta}{r} & \partial_r u_s + \frac{\partial_T u_r + C \cos \theta u_s}{\beta} \\ // & 2\frac{\partial_\theta u_\theta + u_r}{r} & \frac{\partial_\theta u_s}{r} + \frac{\partial_T u_\theta - C \sin \theta u_s}{\beta} \\ // & // & 2\frac{\partial_T u_s - C (\cos \theta u_r - \sin \theta u_\theta)}{\beta} \end{pmatrix}_{e_r, e_\theta, t} \quad (9)$$

Finally, the Navier Stokes equations from Equation (7) in curvilinear coordinates from Equation (8) are

Divergence equation:

$$\frac{1}{r\beta} \partial_r (r\beta u_r) + \frac{1}{r\beta} \partial_\theta (\beta u_\theta) + \frac{1}{r\beta} \partial_T (ru_s) = 0, \quad (10)$$

Radial momentum equation:

$$\begin{aligned}
 & \partial_t u_r + \frac{1}{r\beta} \partial_r (r\beta u_r^2) + \frac{1}{r\beta} \partial_\theta (\beta u_r u_\theta) + \frac{1}{\beta} \partial_T (u_r u_s) + \partial_r p - \frac{u_\theta^2}{r} + \frac{C \cos \theta}{\beta} u_s^2 \\
 &= v \left[\frac{2}{r\beta} \partial_r (r\beta \partial_r u_r) + \frac{1}{r\beta} \partial_\theta \left(\beta \left(\partial_r u_\theta + \frac{\partial_\theta u_r - u_\theta}{r} \right) \right) \right. \\
 & \quad + \frac{1}{r\beta} \partial_T \left(r \left(\partial_r u_s + \frac{\partial_T u_r + C \cos \theta u_s}{\beta} \right) \right) - \frac{2}{r} \frac{\partial_\theta u_\theta + u_r}{r} \\
 & \quad \left. + \frac{C \cos \theta}{\beta} \left(2 \frac{\partial_T u_s - C (\cos \theta u_r - \sin \theta u_\theta)}{\beta} \right) \right] \tag{11}
 \end{aligned}$$

Angular momentum equation:

$$\begin{aligned}
 & \partial_t u_\theta + \frac{1}{r\beta} \partial_r (r\beta u_r u_\theta) + \frac{1}{r\beta} \partial_\theta (\beta u_\theta^2) + \frac{1}{\beta} \partial_T (u_\theta u_s) + \frac{1}{r} \partial_\theta p + \frac{u_\theta u_r}{r} - \frac{C \sin \theta}{\beta} u_s^2 \\
 &= v \left[\frac{1}{r\beta} \partial_r \left(r\beta \left(\partial_r u_\theta + \frac{\partial_\theta u_r - u_\theta}{r} \right) \right) + \frac{2}{r\beta} \partial_\theta \left(\beta \frac{\partial_\theta u_\theta + u_r}{r} \right) \right. \\
 & \quad + \frac{1}{r\beta} \partial_T \left(r \left(\frac{\partial_\theta u_s}{r} + \frac{\partial_T u_\theta - C \sin \theta u_s}{\beta} \right) \right) + \frac{1}{r} \left(\partial_r u_\theta + \frac{\partial_\theta u_r - u_\theta}{r} \right) \\
 & \quad \left. - \frac{C \sin \theta}{\beta} \left(2 \frac{\partial_T u_s - C (\cos \theta u_r - \sin \theta u_\theta)}{\beta} \right) \right] \tag{12}
 \end{aligned}$$

Axial momentum equation:

$$\begin{aligned}
 & \partial_t u_s + \frac{1}{r\beta} \partial_r (r\beta u_r u_s) + \frac{1}{r\beta} \partial_\theta (\beta u_\theta u_s) + \frac{1}{\beta} \partial_T (u_s^2) + \frac{1}{\beta} \partial_T p - \frac{C}{\beta} (u_r \cos \theta - u_\theta \sin \theta) u_s \\
 &= v \left[\frac{1}{r\beta} \partial_r \left(r\beta \left(\partial_r u_s + \frac{\partial_T u_r + C \cos \theta u_s}{\beta} \right) \right) + \frac{1}{r\beta} \partial_\theta \left(\beta \left(\frac{\partial_\theta u_s}{r} + \frac{\partial_T u_\theta - C \sin \theta u_s}{\beta} \right) \right) \right. \\
 & \quad + \frac{1}{r\beta} \partial_T \left(r \left(2 \frac{\partial_T u_s - C (\cos \theta u_r - \sin \theta u_\theta)}{\beta} \right) \right) \\
 & \quad \left. - \frac{C}{\beta} \left(\cos \theta \left(\partial_r u_s + \frac{\partial_T u_r + C \cos \theta u_s}{\beta} \right) - \sin \theta \left(\frac{\partial_\theta u_s}{r} + \frac{\partial_T u_\theta - C \sin \theta u_s}{\beta} \right) \right) \right] \tag{13}
 \end{aligned}$$

2.1.2. The Artery Wall Boundary

Crucial to our model derivation is the particular situation at the wall boundary, where the effect of wall deformation plays a central role. The wall boundary is the set of points

$$\Gamma = \{c(s) + R(t, \theta, s) \mathbf{e}_r(\theta, s) \mid \theta \in [0, 2\pi[, s \in [0, L], t \in [0, T]\}.$$

We define Γ 's tangential and outward normal vectors by

$$\begin{aligned}
 \mathbf{t}_s^w &= \frac{1}{G_s} \left(\mathbf{t} + \frac{\partial_T R}{\beta} \mathbf{e}_r \right), \\
 \mathbf{t}_\theta^w &= \frac{1}{G_\theta} \left(\mathbf{e}_\theta + \frac{\partial_\theta R}{R} \mathbf{e}_r \right), \\
 \mathbf{n}^w &= \frac{1}{G} \left(\mathbf{e}_r - \frac{\partial_\theta R}{R} \mathbf{e}_\theta - \frac{\partial_T R}{\beta} \mathbf{t} \right),
 \end{aligned}$$

where G_s , G_θ and G are the axial, circumferential and normal arclength

$$G_s = \sqrt{1 + \left(\frac{\partial_\tau R}{\beta}\right)^2}, \quad G_\theta = \sqrt{1 + \left(\frac{\partial_\theta R}{R}\right)^2}, \quad G = \sqrt{1 + \left(\frac{\partial_\theta R}{R}\right)^2 + \left(\frac{\partial_\tau R}{\beta}\right)^2}.$$

Since the wall is assumed to be rough, it produces friction, and due to its elastic behavior, it may get deformed. We take friction into account by considering the following Navier boundary condition on the wall Γ ,

$$(\sigma \mathbf{n}^w) \cdot \mathbf{t}_s^w = k \mathbf{u} \cdot \mathbf{t}_s^w, \quad (\sigma \mathbf{n}^w) \cdot \mathbf{t}_\theta^w = k \mathbf{u} \cdot \mathbf{t}_\theta^w, \tag{14}$$

where $k \leq 0$ is a friction term. Fluid-structure interaction is modeled with the condition

$$\mathbf{u} \cdot \mathbf{n}^w = \partial_\tau R \mathbf{e}_r \cdot \mathbf{n}^w. \tag{15}$$

As assumed in [6], thanks to the following hypothesis:

H1 Small thickness and plain stresses: the vessel wall thickness h is assumed to be, a constant, small enough to allow a shell-type representation of the artery geometry. The vessel structure is subjected to plain stresses.

H2 Radial displacement: the artery is described by a star-like cross-section around a curvilinear curve, and its displacements are only in the radial direction.

H3 Small deformation gradients and linear elastic behavior: we suppose that the artery wall behaves like a linear elastic solid where $\partial_\tau R$ and $\partial_\theta R$ are assumed to be bounded in time.

H4 Incompressibility: the wall tissue is incompressible [12].

H5 Dominance of circumferential stresses. Stresses acting along the axial direction can be neglected compared to circumferential ones.

One can derive the wall dynamic law:

$$\partial_t^2 \eta + \frac{\rho}{h \rho_w} b \frac{\eta}{R_0^2} = \frac{R}{R_0} \frac{\rho}{h \rho_w} [p - p_{\text{ext}} - G \sigma \mathbf{n}^w \cdot \mathbf{e}_r], \tag{16}$$

where $\eta = R - R_0$ is the displacement of the wall, $R_0 = R(t=0, \theta, s)$ is the initial radius of the artery, ρ^w is the wall tissues density, h is the wall thickness,

p_{ext} is the external pressure $b(\theta, s) = \frac{E(\theta, s)h}{\rho(1-\xi^2)}$ is a function of the Young

modulus E , σ from Equation (9) is the fluid stress tensor at $r = R$, and p is the fluid pressure at $r = R$.

Remark. These assumptions allow us to properly set the asymptotic regime discussed in the following sections of this paper. More precisely,

H1 implies that the arterial wall thickness can be considered small compared to the artery radius. This assumption holds both for large and small arteries.

H2 represents a fundamental limitation of this model, clearly marking the boundary with 3D models. Nevertheless, it remains far more reasonable than in the 1D case.

H3 can be relaxed, as is often done in the 1D framework; the adaptation to 2D should be similar. However, our objective here is to show that a bidimensional

model with arbitrary friction can still retain energetic consistency with the Navier-Stokes equations. For this reason, we did not include a very detailed arterial wall model. Such a refinement could nonetheless be necessary for complex studies of blood flow in cerebral arteries. Similarly, aneurysm cases might be affected by the absence of hyperelasticity.

H4 is reasonable for a solid such as the arterial wall.

H5 may seem restrictive in light of [6], where the authors show how to avoid it. In our case, the same calculation can also be carried out, and the corresponding term can be added if needed. However, it remains of lower order in the asymptotic expansion presented later in this paper. The derivation of the arterial model is not detailed here, but a complete derivation confirms the asymptotic consistency of the model. We choose to keep the assumption for consistency with [6] but it is a direct consequence of the asymptotic regime.

Gathering Equations (14), (15) and (16), boundary conditions can be written:

Normal boundary condition

$$u_r - \frac{\partial_\theta R}{R} u_\theta - \frac{\partial_T R}{\beta} u_s = \partial_r R, \tag{17}$$

Axial tangential boundary condition

$$\begin{aligned} & \nu \left[\partial_r u_s + \frac{\partial_T u_r + C \cos \theta u_s}{\beta} - \frac{\partial_\theta R}{R} \left(\frac{\partial_\theta u_s}{R} + \frac{\partial_T u_\theta - C \sin \theta u_s}{\beta} \right) \right. \\ & \left. - \frac{\partial_T R}{\beta} \left(2 \frac{\partial_T u_s - C(\cos \theta u_r - \sin \theta u_\theta)}{\beta} \right) \right. \\ & \left. + \frac{\partial_T R}{\beta} \left(2 \partial_r u_r - \frac{\partial_\theta R}{R} \left(\partial_r u_\theta + \frac{\partial_\theta u_r - u_\theta}{R} \right) - \frac{\partial_T R}{\beta} \left(\partial_r u_s + \frac{\partial_T u_r + C \cos \theta u_s}{\beta} \right) \right) \right] \tag{18} \\ & = Gk \left(u_s + \frac{\partial_T R}{\beta} u_r \right), \end{aligned}$$

Angular tangential boundary condition

$$\begin{aligned} & \nu \left[\partial_r u_\theta + \frac{\partial_\theta u_r - u_\theta}{R} - \frac{\partial_\theta R}{R} \left(2 \frac{\partial_\theta u_\theta + u_r}{R} \right) - \frac{\partial_T R}{\beta} \left(\frac{\partial_\theta u_s}{R} + \frac{\partial_T u_\theta - C \sin \theta u_s}{\beta} \right) \right. \\ & \left. + \frac{\partial_\theta R}{R} \left(2 \partial_r u_r - \frac{\partial_\theta R}{R} \left(\partial_r u_\theta + \frac{\partial_\theta u_r - u_\theta}{R} \right) - \frac{\partial_T R}{\beta} \left(\partial_r u_s + \frac{\partial_T u_r + C \cos \theta u_s}{\beta} \right) \right) \right] \tag{19} \\ & = Gk \left(u_\theta + \frac{\partial_\theta R}{R} u_r \right), \end{aligned}$$

Wall dynamic law

$$\begin{aligned} & \frac{h \rho_w R_0}{\rho R} \partial_r^2 R + b \frac{R - R_0}{RR_0} \\ & + \nu \left[2 \partial_r u_r - \frac{\partial_\theta R}{R} \left(\partial_r u_\theta + \frac{\partial_\theta u_r - u_\theta}{R} \right) - \frac{\partial_T R}{\beta} \left(\partial_r u_s + \frac{\partial_T u_r + C \cos \theta u_s}{\beta} \right) \right] \tag{20} \\ & = p - p_{ext}. \end{aligned}$$

2.2. Blood Flow Model with Wall Deformation via Radial-Averaging

We now proceed to write the Navier-Stokes equations with boundary conditions in non-dimensional form. Next, under a thin-artery assumption, we consider the radius of the artery to be small compared to the length, introducing a small parameter ε . This assumption may be rather restrictive for large arteries. However, it has been shown that a similarly derived one-dimensional model remains effective in such cases [6]. The applicability of our model to strongly deformed arteries requires thorough testing in order to properly define its range of validity. Such a study lies beyond the scope of this paper, since our focus here is on the model derivation and its energetic consistency rather than on an exhaustive validation.

We formally make an asymptotic expansion of the Navier-Stokes system in first order with respect to ε . Finally, we derive a radial-averaged first-order two-dimensional model for blood flow. Our approach is similar to those used in [6] [14]-[16] [19].

2.2.1. Dimensionless Navier-Stokes Equations

To derive the blood flow model, we assume that the artery's radius is small compared to its length and that radial variations in velocity are small compared to axial ones. This is achieved by postulating a small parameter ratio

$$\varepsilon := \frac{\bar{R}}{L} = \frac{U_r}{U_s} = \frac{U_r}{U_\theta} \ll 1,$$

where, \bar{R} , L , U_r , U_θ , and U_s are the scales of, respectively, radius, length, radial velocity, angular velocity, and axial velocity. As a consequence, the time scale T is such that $T = \frac{L}{U_s} = \frac{L}{U_\theta} = \frac{\bar{R}}{U_r}$. We also choose the pressure scale to be

$$\bar{p} = U_s^2 = U_\theta^2. \quad (21)$$

It is convenient to define L, U_s, U_θ and T , as finite constants with respect to ε , while $\bar{R} = \varepsilon L$ and $U_r = \varepsilon U_s = \varepsilon U_\theta$. This allows us to introduce the dimensionless quantities of time \tilde{t} , space $(\tilde{s}, \tilde{r}, \tilde{\theta})$, pressure \tilde{p} and velocity field $(\tilde{u}_s, \tilde{u}_\theta, \tilde{u}_r)$ via the following scaling relations

$$\begin{aligned} \tilde{t} &:= \frac{t}{T}, & \tilde{p}(\tilde{t}, \tilde{r}, \tilde{\theta}, \tilde{s}) &= \frac{p(t, r, \theta, s)}{\bar{p}}, \\ \tilde{s} &:= \frac{s}{L}, & \tilde{u}_s(\tilde{t}, \tilde{r}, \tilde{\theta}, \tilde{s}) &= \frac{u_s(t, r, \theta, s)}{U_s}, \\ \tilde{r} &:= \frac{r}{\bar{R}} = \frac{r}{\varepsilon L}, & \tilde{u}_r(\tilde{t}, \tilde{r}, \tilde{\theta}, \tilde{s}) &= \frac{u_r(t, r, \theta, s)}{U_r}, \\ \tilde{\theta} &:= \frac{\theta}{\varepsilon}, & \tilde{u}_\theta(\tilde{t}, \tilde{r}, \tilde{\theta}, \tilde{s}) &= \frac{u_\theta(t, r, \theta, s)}{U_\theta}. \end{aligned} \quad (22)$$

We also rescale the following coefficients

$$\begin{aligned} \tilde{k} &= \frac{k}{U_r} = \frac{k}{\varepsilon U_s} = \frac{k}{\varepsilon U_\theta}, & \tilde{R}(\tilde{r}, \tilde{\theta}, \tilde{s}) &= \frac{R(t, \theta, s)}{\bar{R}}, \\ \tilde{h} &= \frac{h}{\varepsilon \bar{R}}, & \tilde{E}(\tilde{\theta}, \tilde{s}) &= \varepsilon \frac{E(\theta, s)}{\rho U_s^2}, \\ \tilde{R}_0(\tilde{\theta}, \tilde{s}) &= \frac{R_0(\theta, s)}{\bar{R}} & \tilde{C}(\tilde{s}) &= LC(s) \\ \tilde{T}(\tilde{s}) &= LT(s). \end{aligned} \tag{23}$$

Finally, we define the non-dimensional Reynolds number $R_e = \frac{LU_s}{\nu}$ and $\nu_0 = (\varepsilon R_e)^{-1}$ yielding to the asymptotic regime

$$R_e^{-1} = \nu_0 \varepsilon. \tag{24}$$

Let us also remark that

$$\begin{aligned} \beta(\tilde{r}, \tilde{\theta}, \tilde{s}) &= 1 - \varepsilon \tilde{r} \tilde{C} \cos \theta = 1 + O(\varepsilon) \\ \text{and } \partial_{\tilde{T}} &= \frac{1}{L} \partial_{\tilde{T}} = \frac{1}{L} (\partial_{\tilde{s}} - \varepsilon \tilde{T} \partial_{\tilde{\theta}}) = \frac{1}{L} \partial_{\tilde{s}} + O(\varepsilon). \end{aligned}$$

With these assumptions, the effect of torsion is neglected.

Using these dimensionless variables, Equations (21)-(24) in the Navier-Stokes equations from Equations (10)-(13), we get

Dimensionless divergence equation:

$$\frac{1}{\tilde{r} \tilde{\beta}} \partial_{\tilde{r}} (\tilde{r} \tilde{\beta} \tilde{u}_r) + \frac{1}{\tilde{r} \tilde{\beta}} \partial_{\tilde{\theta}} (\tilde{\beta} \tilde{u}_\theta) + \frac{1}{\tilde{\beta}} \partial_{\tilde{T}} (\tilde{u}_s) = 0, \tag{25}$$

Dimensionless radial momentum equation:

$$\partial_{\tilde{r}} \tilde{p} - \frac{\tilde{u}_\theta^2}{\tilde{r}} = \varepsilon \delta_{r\varepsilon}, \tag{26}$$

with

$$\begin{aligned} \delta_{r\varepsilon} &= \varepsilon \left[\partial_{\tilde{r}} \tilde{u}_r + \frac{1}{\tilde{r} \tilde{\beta}} \partial_{\tilde{r}} (\tilde{r} \tilde{\beta} \tilde{u}_r^2) + \frac{1}{\tilde{r} \tilde{\beta}} \partial_{\tilde{\theta}} (\tilde{\beta} \tilde{u}_r \tilde{u}_\theta) + \frac{1}{\tilde{\beta}} \partial_{\tilde{T}} (\tilde{u}_r \tilde{u}_s) \right] + \frac{\tilde{C} \cos \tilde{\theta}}{\tilde{\beta}} \tilde{u}_s^2 \\ &- \nu_0 \left[\frac{2}{\tilde{r} \tilde{\beta}} \partial_{\tilde{r}} (\tilde{r} \tilde{\beta} \partial_{\tilde{r}} \tilde{u}_r) + \frac{1}{\tilde{r} \tilde{\beta}} \partial_{\tilde{\theta}} \left(\tilde{\beta} \left(\partial_{\tilde{r}} \tilde{u}_\theta + \frac{\varepsilon^2 \partial_{\tilde{\theta}} \tilde{u}_r - \tilde{u}_\theta}{\tilde{r}} \right) \right) - \frac{2}{\tilde{r}} \frac{\partial_{\tilde{\theta}} \tilde{u}_\theta + \tilde{u}_r}{\tilde{r}} \right. \\ &+ \frac{1}{\tilde{r} \tilde{\beta}} \partial_{\tilde{T}} \left(\tilde{r} \left(\partial_{\tilde{r}} \tilde{u}_s + \frac{\varepsilon^2 \partial_{\tilde{T}} \tilde{u}_r + \varepsilon \tilde{C} \cos \tilde{\theta} \tilde{u}_s}{\tilde{\beta}} \right) \right) \\ &\left. + \varepsilon \frac{\tilde{C} \cos \tilde{\theta}}{\tilde{\beta}} \left(2 \frac{\partial_{\tilde{T}} \tilde{u}_s - \tilde{C} (\varepsilon \cos \tilde{\theta} \tilde{u}_r - \sin \tilde{\theta} \tilde{u}_\theta)}{\tilde{\beta}} \right) \right] \end{aligned}$$

Dimensionless angular momentum equation:

$$\begin{aligned} \partial_{\tilde{r}} \tilde{u}_\theta + \frac{1}{\tilde{r} \tilde{\beta}} \partial_{\tilde{r}} (\tilde{r} \tilde{\beta} \tilde{u}_r \tilde{u}_\theta) + \frac{1}{\tilde{r} \tilde{\beta}} \partial_{\tilde{\theta}} (\tilde{\beta} \tilde{u}_\theta^2) + \frac{1}{\tilde{\beta}} \partial_{\tilde{T}} (\tilde{u}_\theta \tilde{u}_s) + \frac{1}{\tilde{r}} \partial_{\tilde{\theta}} \tilde{p} + \frac{\tilde{u}_\theta \tilde{u}_r}{\tilde{r}} \\ - \frac{\tilde{C} \sin \tilde{\theta}}{\tilde{\beta}} \tilde{u}_s^2 = \frac{1}{\varepsilon} \nu_0 \left[\frac{1}{\tilde{r} \tilde{\beta}} \partial_{\tilde{r}} \left(\tilde{r} \tilde{\beta} \left(\partial_{\tilde{r}} \tilde{u}_\theta - \frac{\tilde{u}_\theta}{\tilde{r}} \right) \right) + \frac{\partial_{\tilde{r}} \tilde{u}_\theta - \tilde{u}_\theta}{\tilde{r}^2} \right] + \varepsilon \delta_{\theta\varepsilon}, \end{aligned} \tag{27}$$

with

$$\begin{aligned} \delta_{\theta\epsilon} = v_0 & \left[\frac{1}{\tilde{r}\tilde{\beta}} \partial_{\tilde{r}} \left(\tilde{r}\tilde{\beta} \left(\frac{\partial_{\tilde{\theta}} \tilde{u}_r}{\tilde{r}} \right) \right) + \frac{2}{\tilde{r}\tilde{\beta}} \partial_{\tilde{\theta}} \left(\tilde{\beta} \frac{\partial_{\tilde{\theta}} \tilde{u}_\theta + \tilde{u}_r}{\tilde{r}} \right) \right. \\ & + \frac{1}{\tilde{r}\tilde{\beta}} \partial_{\tilde{r}} \left(\tilde{r} \left(\frac{\partial_{\tilde{\theta}} \tilde{u}_s}{\tilde{r}} + \frac{\partial_{\tilde{r}} \tilde{u}_\theta - \tilde{C} \sin \tilde{\theta} \tilde{u}_s}{\tilde{\beta}} \right) \right) \\ & \left. + \frac{1}{\tilde{r}} \left(\frac{\partial_{\tilde{\theta}} \tilde{u}_r}{\tilde{r}} \right) - \frac{\tilde{C} \sin \tilde{\theta}}{\tilde{\beta}} \left(2 \frac{\partial_{\tilde{r}} \tilde{u}_s - \tilde{C} (\epsilon \cos \tilde{\theta} \tilde{u}_r - \sin \tilde{\theta} \tilde{u}_\theta)}{\tilde{\beta}} \right) \right] \end{aligned}$$

Dimensionless axial momentum equation:

$$\begin{aligned} \partial_{\tilde{r}} \tilde{u}_s + \frac{1}{\tilde{r}\tilde{\beta}} \partial_{\tilde{r}} (\tilde{r}\tilde{\beta} \tilde{u}_r \tilde{u}_s) + \frac{1}{\tilde{r}\tilde{\beta}} \partial_{\tilde{\theta}} (\tilde{\beta} \tilde{u}_\theta \tilde{u}_s) + \frac{1}{\tilde{\beta}} \partial_{\tilde{r}} (\tilde{u}_s^2) + \frac{1}{\tilde{\beta}} \partial_{\tilde{r}} \tilde{p} + \frac{\tilde{C} \sin \tilde{\theta}}{\tilde{\beta}} \tilde{u}_\theta \tilde{u}_s \\ = \frac{v_0}{\epsilon} \left[\frac{1}{\tilde{r}\tilde{\beta}} \partial_{\tilde{r}} (\tilde{r}\tilde{\beta} \partial_{\tilde{r}} \tilde{u}_s) - \epsilon \frac{\tilde{C}}{\tilde{r}\tilde{\beta}} \cos \tilde{\theta} \tilde{u}_s \right] + \epsilon \delta_{se}, \end{aligned} \tag{28}$$

with

$$\begin{aligned} \delta_{se} = \frac{\tilde{C} \cos \tilde{\theta}}{\tilde{\beta}} \tilde{u}_r \tilde{u}_s + v_0 & \left[\frac{1}{\tilde{r}\tilde{\beta}} \partial_{\tilde{r}} (\tilde{r} \partial_{\tilde{r}} \tilde{u}_r) + \frac{1}{\tilde{r}\tilde{\beta}} \partial_{\tilde{\theta}} \left(\tilde{\beta} \left(\frac{\partial_{\tilde{\theta}} \tilde{u}_s}{\tilde{r}} + \frac{\partial_{\tilde{r}} \tilde{u}_\theta - \tilde{C} \sin \tilde{\theta} \tilde{u}_s}{\tilde{\beta}} \right) \right) \right. \\ & + \frac{1}{\tilde{r}\tilde{\beta}} \partial_{\tilde{r}} \left(\tilde{r} \left(2 \frac{\partial_{\tilde{r}} \tilde{u}_s - \tilde{C} (\epsilon \cos \tilde{\theta} \tilde{u}_r - \sin \tilde{\theta} \tilde{u}_\theta)}{\tilde{\beta}} \right) \right) \\ & \left. - \frac{\tilde{C}}{\tilde{\beta}} \left(\cos \tilde{\theta} \left(\frac{\epsilon \partial_{\tilde{r}} \tilde{u}_r + \tilde{C} \cos \tilde{\theta} \tilde{u}_s}{\tilde{\beta}} \right) - \sin \tilde{\theta} \left(\frac{\partial_{\tilde{\theta}} \tilde{u}_s}{\tilde{r}} + \frac{\partial_{\tilde{r}} \tilde{u}_\theta - \tilde{C} \sin \tilde{\theta} \tilde{u}_s}{\tilde{\beta}} \right) \right) \right]. \end{aligned}$$

Similarly, the boundary conditions from Equations (17)-(20) become

Dimensionless normal boundary condition

$$\tilde{u}_r - \frac{\partial_{\tilde{\theta}} \tilde{R}}{\tilde{R}} \tilde{u}_\theta - \frac{\partial_{\tilde{r}} \tilde{R}}{\tilde{\beta}} \tilde{u}_s = \partial_{\tilde{r}} \tilde{R}, \tag{29}$$

Dimensionless axial tangential boundary condition

$$v_0 \partial_{\tilde{r}} \tilde{u}_s = \epsilon \left(\tilde{G} \tilde{k} \tilde{u}_s - v_0 \frac{\tilde{C} \cos \tilde{\theta}}{\tilde{\beta}} \tilde{u}_s \right) + \epsilon^2 \delta_{Rse}, \tag{30}$$

with,

$$\begin{aligned} \delta_{Rse} = -v_0 & \left[\frac{\partial_{\tilde{r}} \tilde{u}_r}{\tilde{\beta}} - \frac{\partial_{\tilde{\theta}} \tilde{R}}{\tilde{R}} \left(\frac{\partial_{\tilde{\theta}} \tilde{u}_s}{\tilde{R}} + \frac{\partial_{\tilde{r}} \tilde{u}_\theta - \tilde{C} \sin \tilde{\theta} \tilde{u}_s}{\tilde{\beta}} \right) \right. \\ & - \frac{\partial_{\tilde{r}} \tilde{R}}{\tilde{\beta}} \left(2 \frac{\partial_{\tilde{r}} \tilde{u}_s - \tilde{C} (\epsilon \cos \tilde{\theta} \tilde{u}_r - \sin \tilde{\theta} \tilde{u}_\theta)}{\tilde{\beta}} \right) \\ & + \frac{\partial_{\tilde{r}} \tilde{R}}{\tilde{\beta}} \left(2 \partial_{\tilde{r}} \tilde{u}_r - \frac{\partial_{\tilde{\theta}} \tilde{R}}{\tilde{R}} \left(\epsilon^2 \partial_{\tilde{r}} \tilde{u}_\theta + \frac{\partial_{\tilde{\theta}} \tilde{u}_r - \tilde{u}_\theta}{\tilde{R}} \right) \right. \\ & \left. \left. - \frac{\partial_{\tilde{r}} \tilde{R}}{\tilde{\beta}} \left(\partial_{\tilde{r}} \tilde{u}_s + \frac{\epsilon^2 \partial_{\tilde{r}} \tilde{u}_r + \epsilon \tilde{C} \cos \tilde{\theta} \tilde{u}_s}{\tilde{\beta}} \right) \right) \right] + \tilde{G} \tilde{k} \frac{\partial_{\tilde{r}} \tilde{R}}{\tilde{\beta}} \tilde{u}_r, \end{aligned}$$

Dimensionless angular tangential boundary condition

$$v_0 \left[\partial_{\tilde{r}} \tilde{u}_\theta - \frac{\tilde{u}_\theta}{\tilde{R}} \right] = \varepsilon \tilde{k} \tilde{u}_\theta + \varepsilon^2 \delta_{R\theta\varepsilon}, \tag{31}$$

with

$$\begin{aligned} \delta_{R\theta\varepsilon} = & -v_0 \left[\frac{\partial_{\tilde{\theta}} \tilde{u}_r}{\tilde{R}} - \frac{\partial_{\tilde{\theta}} \tilde{R}}{\tilde{R}} \left(2 \frac{\partial_{\tilde{\theta}} \tilde{u}_\theta + \tilde{u}_r}{\tilde{R}} \right) - \frac{\partial_{\tilde{r}} \tilde{R}}{\tilde{\beta}} \left(\frac{\partial_{\tilde{\theta}} \tilde{u}_s}{\tilde{R}} + \frac{\partial_{\tilde{r}} \tilde{u}_\theta - \tilde{C} \sin \tilde{\theta} \tilde{u}_s}{\tilde{\beta}} \right) \right. \\ & + \frac{\partial_{\tilde{\theta}} \tilde{R}}{\tilde{R}} \left(2 \partial_{\tilde{r}} \tilde{u}_r - \frac{\partial_{\tilde{\theta}} \tilde{R}}{\tilde{R}} \left(\partial_{\tilde{r}} \tilde{u}_\theta + \frac{\varepsilon^2 \partial_{\tilde{\theta}} \tilde{u}_r - \tilde{u}_\theta}{\tilde{R}} \right) \right. \\ & \left. \left. - \frac{\partial_{\tilde{r}} \tilde{R}}{\tilde{\beta}} \left(\partial_{\tilde{r}} \tilde{u}_s + \frac{\varepsilon^2 \partial_{\tilde{r}} \tilde{u}_r + \varepsilon \tilde{C} \cos \tilde{\theta} \tilde{u}_s}{\tilde{\beta}} \right) \right) \right] + \tilde{G} \tilde{k} \frac{\partial_{\tilde{\theta}} \tilde{R}}{\tilde{R}} \tilde{u}_r, \end{aligned}$$

Dimensionless wall dynamic law

$$\tilde{b} \frac{\tilde{R} - \tilde{R}_0}{\tilde{R} \tilde{R}_0} = \tilde{p} - \tilde{p}_{ext} + \varepsilon \delta_{R\varepsilon}, \tag{32}$$

with,

$$\begin{aligned} \delta_{R\varepsilon} = & -\varepsilon^2 \frac{\tilde{h} \rho_w}{\rho} \frac{\tilde{R}_0}{\tilde{R}} \partial_{\tilde{r}}^2 \tilde{R} - v_0 \left[2 \partial_{\tilde{r}} \tilde{u}_r - \frac{\partial_{\tilde{\theta}} \tilde{R}}{\tilde{R}} \left(\partial_{\tilde{r}} \tilde{u}_\theta + \frac{\varepsilon^2 \partial_{\tilde{\theta}} \tilde{u}_r - \tilde{u}_\theta}{\tilde{R}} \right) \right. \\ & \left. - \frac{\partial_{\tilde{r}} \tilde{R}}{\tilde{\beta}} \left(\partial_{\tilde{r}} \tilde{u}_s + \frac{\varepsilon^2 \partial_{\tilde{r}} \tilde{u}_r + \varepsilon \tilde{C} \cos \tilde{\theta} \tilde{u}_s}{\tilde{\beta}} \right) \right] \end{aligned}$$

where $\tilde{b}(\tilde{\theta}, \tilde{s}) = \frac{\tilde{E}(\tilde{\theta}, \tilde{s}) h}{1 - \varepsilon^2}$.

2.2.2. First Order Approximation of the Dimensionless Navier-Stokes Equations

In the following, we omit the \tilde{r} . Identifying terms of order $\frac{1}{\varepsilon}$ in the axial momentum Equation (28), we obtain the *motion by radius* (similar to the so-called *motion by slices*, see [13]-[16]) decomposition

$$v_0 \frac{1}{r} \partial_r (r \partial_r u_s) = O(\varepsilon) \Rightarrow r \partial_r u_s = O(\varepsilon) \Rightarrow u_s(t, r, \theta, s) = u_{s,0}(t, \theta, s) + O(\varepsilon),$$

for some function $u_{s,0}$ and where we gathered all ε terms in $O(\varepsilon)$. Similarly,

identifying terms of order $\frac{1}{\varepsilon}$ in the angular momentum Equation (27), we obtain the motion by radial decomposition

$$\begin{aligned} v_0 \left[\frac{1}{r \beta} \partial_r \left(r \beta \left(\partial_r u_\theta - \frac{u_\theta}{r} \right) \right) + \frac{\partial_r u_\theta}{r} - \frac{u_\theta}{r^2} \right] &= O(\varepsilon), \\ \Rightarrow v_0 \left[\frac{1}{r} \partial_r \left(r^2 \partial_r \left(\frac{u_\theta}{r} \right) \right) + \partial_r \left(\frac{u_\theta}{r} \right) \right] &= O(\varepsilon). \\ \Rightarrow v_0 \left[\partial_r \left(r \partial_r \left(\frac{u_\theta}{r} \right) + 2 \frac{u_\theta}{r} \right) \right] &= O(\varepsilon). \end{aligned}$$

Using the angular tangential boundary condition from Equation (31), it is straightforward to see that the only solution is,

$$\frac{u_\theta}{r} = \left(\frac{u_\theta}{r} \right) (r = R) + O(\varepsilon).$$

Noting

$$\begin{aligned} \overline{u_s}(t, \theta, s) &= \frac{1}{A(t, \theta, s)} \int_0^{R(t, \theta, s)} r u_s(t, r, \theta, s) dr, \\ \overline{u_\theta}(t, \theta, s) &= \frac{1}{A(t, \theta, s)} \int_0^R r u_\theta(t, r, \theta, s) dr, \end{aligned}$$

as the mean axial and angular speeds of the fluid over a radius where

$$A(t, \theta, s) = \frac{R^2(t, \theta, s)}{2}, \quad (33)$$

we have the following properties:

$$u_s(t, r, \theta, s) = \overline{u_s}(t, \theta, s) + O(\varepsilon) \quad \text{and} \quad \overline{u_s^2}(t, r, \theta, s) = \overline{u_s}^2(t, \theta, s) + O(\varepsilon), \quad (34)$$

$$u_\theta(t, r, \theta, s) = \frac{3}{2} \overline{u_\theta}(t, \theta, s) \frac{r}{R} + O(\varepsilon) \quad \text{and} \quad \overline{u_\theta^2}(t, r, \theta, s) = \frac{9}{8} \overline{u_\theta}^2(t, \theta, s) + O(\varepsilon). \quad (35)$$

Multiplying by r and integrating the divergence Equation (25) over a radius, we obtain

$$\begin{aligned} 0 &= \int_0^R \left[\partial_r (r u_r) + \partial_\theta (u_\theta) + \partial_s (r u_s) \right] + O(\varepsilon) \\ &= R u_r(r = R) + \partial_\theta \left(\int_0^R u_\theta dr \right) - \partial_\theta R u_\theta(r = R) \\ &\quad + \partial_s \left(\int_0^R r u_s dr \right) - \partial_s R R u_s(r = R) + O(\varepsilon). \end{aligned}$$

In view of the normal boundary condition from Equation (29), we get the conservation equation

$$\partial_r A + \partial_\theta \left(\frac{3}{2} \frac{Q_\theta}{R} \right) + \partial_s (Q_s) = O(\varepsilon), \quad (36)$$

where,

$$\begin{aligned} Q_\theta(t, \theta, s) &= A(t, \theta, s) \overline{u_\theta}(t, \theta, s) = \int_0^R r u_\theta dr, \\ Q_s(t, \theta, s) &= A(t, \theta, s) \overline{u_s}(t, \theta, s) = \int_0^R r u_s dr. \end{aligned} \quad (37)$$

Then, integrating the radial momentum Equation (26) between r and R , we obtain the following pressure

$$\begin{aligned} p(t, r, \theta, s) &= p(t, R, \theta, s) - \int_r^R \frac{u_\theta^2}{s} ds + O(\varepsilon) \\ &= p(t, R, \theta, s) - \frac{9}{8} \frac{Q_\theta^2}{A^2} \left(1 - \left(\frac{r}{R} \right)^2 \right) + O(\varepsilon) \end{aligned} \quad (38)$$

We proceed with multiplying by r^2 and integrating over a radius the angular momentum Equation (27)

$$\int_0^R r^2 \left[\partial_t u_\theta + \frac{1}{r} \partial_r (ru_r u_\theta) + \frac{1}{r} \partial_\theta (u_\theta^2) + \partial_s (u_\theta u_s) + \frac{1}{r} \partial_\theta p + \frac{u_\theta u_r}{r} - C \sin \theta u_s^2 \right] dr$$

$$= \int_0^R r^2 \left[\frac{1}{\varepsilon} v_0 \left[\frac{1}{r} \partial_r \left(r \left(\partial_r u_\theta - \frac{u_\theta}{r} \right) \right) + \frac{\partial_r u_\theta}{r} - \frac{u_\theta}{r^2} \right] \right] dr + O(\varepsilon),$$

yielding to

$$\int_0^R r^2 \partial_t u_\theta + \int_0^R \partial_r (r^2 u_r u_\theta) + \int_0^R \partial_\theta (ru_\theta^2) + \int_0^R \partial_s (r^2 u_\theta u_s) + \int_0^R \partial_\theta (rp)$$

$$- C \sin \theta \int_0^R r^2 u_s^2 = \int_0^R \left[\frac{1}{\varepsilon} v_0 \left[r \partial_r \left(r^2 \partial_r \left(\frac{u_\theta}{r} \right) \right) + r^2 \partial_r \left(\frac{u_\theta}{r} \right) \right] \right] + O(\varepsilon),$$

and then,

$$\int_0^R r^2 \partial_t u_\theta + \int_0^R \partial_r (r^2 u_r u_\theta) + \int_0^R \partial_\theta (ru_\theta^2) + \int_0^R \partial_s (r^2 u_\theta u_s) + \int_0^R \partial_\theta (rp)$$

$$- C \sin \theta \int_0^R r^2 u_s^2 = \int_0^R \partial_r \left[\frac{1}{\varepsilon} v_0 \left[r^3 \partial_r \left(\frac{u_\theta}{r} \right) \right] \right] + O(\varepsilon),$$

Using the definitions of A in Equation (33), Q_θ and Q_s in Equation (37), thanks to the normal boundary condition from Equation (29), we have

$$\partial_t \left(\int_0^R r^2 u_\theta \right) + \partial_\theta \left(\int_0^R ru_\theta^2 \right) + \partial_s \left(\int_0^R r^2 u_\theta u_s \right) + \partial_\theta \left(\int_0^R rp \right) - \partial_\theta Ap(r=R)$$

$$- C \sin \theta \int_0^R r^2 u_s^2 = \frac{1}{\varepsilon} v_0 \left[R^2 \frac{\varepsilon}{v_0} k u_\theta(r=R) \right] + O(\varepsilon),$$

Then, using the properties from Equation (34) and Equation (35), the expression of the pressure in Equation (38) and the angular tangential boundary condition in Equation (31), we obtain

$$\partial_t \left(\frac{3R}{4} Q_\theta \right) + \partial_\theta \left(\frac{9R}{8} \frac{Q_\theta^2}{RA} \right) + \partial_s \left(\frac{3R}{4} \frac{Q_\theta Q_s}{A} \right) + \partial_\theta \left(Ap(r=R) - \frac{9R}{16} \frac{Q_\theta^2}{RA} \right)$$

$$- \partial_\theta Ap(r=R) - \frac{2R}{3} C \sin \theta \frac{Q_s^2}{A} = \frac{3R}{2} Rk \frac{Q_\theta}{A} + O(\varepsilon), \tag{39}$$

Finally, multiplying by r and integrating over a radius the axial momentum Equation (28)

$$\int_0^R r \left[\partial_t u_s + \frac{1}{r} \partial_r (ru_r u_s) + \frac{1}{r} \partial_\theta (u_\theta u_s) + \partial_s (u_s^2) + \partial_s p + C \sin \theta u_\theta u_s \right] dr$$

$$= \int_0^R r \left[\frac{v_0}{\varepsilon} \left[\frac{1}{r\beta} \partial_r (r\beta \partial_r u_s) + \varepsilon \frac{C \cos \theta}{r} u_s \right] \right] dr + O(\varepsilon),$$

we get

$$\int_0^R \partial_t (ru_s) + Ru_r(r=R)u_s(r=R) + \int_0^R \partial_\theta (u_\theta u_s) + \int_0^R \partial_s (ru_s^2) + \int_0^R \partial_s (rp)$$

$$+ C \sin \theta \int_0^R ru_\theta u_s = \int_0^R r \left[\frac{v_0}{\varepsilon} \left[\frac{1}{r\beta} \partial_r (r\beta \partial_r u_s) + \varepsilon \frac{C \cos \theta}{r} u_s \right] \right] dr + O(\varepsilon),$$

Using the definitions of A from Equation (33), Q_θ and Q_s from Equation (37), thanks to the normal boundary condition in Equation (29), we have

$$\begin{aligned} & \partial_t(Q_s) + \partial_\theta \left(\int_0^R u_\theta u_s \right) + \partial_s \left(\int_0^R r u_s^2 \right) + \partial_s \left(\int_0^R r p \right) - \partial_s A p(r=R) + C \sin \theta \int_0^R r u_\theta u_s \\ & = \frac{V_0}{\varepsilon} \left[R(\partial_r u_s)(r=R) + \int_0^R \frac{\partial_r \beta}{\beta} r \partial_r u_s + \varepsilon C \cos \theta \int_0^R u_s \right] + O(\varepsilon), \end{aligned}$$

Then, using the properties from Equation (34) and Equation (35), the expression of the pressure in Equation (38) and the axial tangential boundary condition in Equation (30), we obtain

$$\begin{aligned} & \partial_t(Q_s) + \partial_\theta \left(\frac{3 Q_s Q_\theta}{2 AR} \right) + \partial_s \left(\frac{Q_s^2}{A} \right) + \partial_s \left(A p(r=R) - \frac{9 Q_\theta^2}{16 A} \right) - \partial_s A p(r=R) \\ & = kR \frac{Q_s}{A} - C \sin \theta \frac{Q_s Q_\theta}{A} + O(\varepsilon), \end{aligned}$$

leading to

$$\begin{aligned} & \partial_t(Q_s) + \partial_\theta \left(\frac{3 Q_s Q_\theta}{2 AR} \right) + \partial_s \left(\frac{Q_s^2}{A} - \frac{9 Q_\theta^2}{16 A} + A p(r=R) \right) \\ & = kR \frac{Q_s}{A} - C \sin \theta \frac{Q_s Q_\theta}{A} + \partial_s A p(r=R) + O(\varepsilon). \end{aligned} \tag{40}$$

Finally from Equations (36), (39), (40) and the wall dynamic law in Equation (32) dropping all terms of the first order, we obtain the following radial-averaged two-dimensional model for blood flow

$$\begin{cases} \partial_t A + \partial_\theta \left(\frac{3 Q_\theta}{2 R} \right) + \partial_s(Q_s) = 0, \\ \partial_t \left(\frac{3R}{4} Q_\theta \right) + \partial_\theta \left(\frac{9R}{16} \frac{Q_\theta^2}{RA} + A p \right) + \partial_s \left(\frac{3R}{4} \frac{Q_\theta Q_s}{A} \right) = \frac{2R}{3} C \sin \theta \frac{Q_s^2}{A} + \frac{3R}{2} R k \frac{Q_\theta}{A} + \partial_\theta A p, \\ \partial_t(Q_s) + \partial_\theta \left(\frac{3 Q_s Q_\theta}{2 AR} \right) + \partial_s \left(\frac{Q_s^2}{A} - \frac{9 Q_\theta^2}{16 A} + A p \right) = kR \frac{Q_s}{A} - C \sin \theta \frac{Q_s Q_\theta}{A} + \partial_s A p, \\ p = p_{ext} + b \frac{R - R_0}{R_0^2}. \end{cases}$$

where we have replaced $p(r=R=\sqrt{2A})$ by p for simplicity. Lastly, using a simple change of variable $Q_{R\theta} = \frac{3}{4} R Q_\theta$, we get,

$$\begin{cases} \partial_t A + \partial_\theta \left(\frac{Q_{R\theta}}{A} \right) + \partial_s(Q_s) = 0, \\ \partial_t(Q_{R\theta}) + \partial_\theta \left(\frac{Q_{R\theta}^2}{2A^2} + A p \right) + \partial_s \left(\frac{Q_{R\theta} Q_s}{A} \right) = \frac{2R}{3} C \sin \theta \frac{Q_s^2}{A} + 2Rk \frac{Q_{R\theta}}{A} + \partial_\theta A p, \\ \partial_t(Q_s) + \partial_\theta \left(\frac{Q_s Q_{R\theta}}{A^2} \right) + \partial_s \left(\frac{Q_s^2}{A} - \frac{Q_{R\theta}^2}{2A^2} + A p \right) = -\frac{2R}{3} C \sin \theta \frac{Q_s Q_{R\theta}}{A^2} + kR \frac{Q_s}{A} + \partial_s A p, \\ p = p_{ext} + b \frac{R - R_0}{R_0^2}. \end{cases} \tag{41}$$

2.2.3. Mathematical Properties for the Two-Dimensional Model

We have the following results

Theorem 1. Let $(A, \bar{u}_\theta, \bar{u}_s)$, and $Q_{R\theta} = \frac{3}{4}RQ_\theta = \frac{3}{4}RA\bar{u}_\theta$, $Q_s = A\bar{u}_s$ satisfy the two-dimensional blood flow system in Equation (41). Then, we have:

1) System (41) is strictly hyperbolic if $A > 0$ and $Ap'(A) - \frac{9}{8}\bar{u}_\theta^{-2} \neq 0$.

2) For smooth solution $(A, \bar{u}_\theta, \bar{u}_s)$, in the region where $A > 0$, we have the following head equation,

$$\partial_t \psi + \frac{3}{2} \frac{\bar{u}_\theta}{R} \partial_\theta (\psi + \bar{p}) + \bar{u}_s \partial_s (\psi + \bar{p}) + \frac{p - \bar{p}}{A} \partial_t A = \frac{9}{4A} Rk\bar{u}_\theta^{-2} + \frac{1}{A} kR\bar{u}_s^{-2}. \quad (42)$$

where $\psi(u_\theta, u_s, p) = \frac{9}{8} \frac{u_\theta^2 + u_s^2}{2}$ is the total head and $\bar{p} = p - \frac{9}{16} \bar{u}_\theta^{-2}$ is the mean pressure over a radius.

3) For smooth solution $(A, \bar{u}_\theta, \bar{u}_s)$, the steady state reads $\bar{u}_\theta = 0$, $\bar{u}_s = 0$ and $p = p_0$ for some constant p_0 . In particular, for $A = A_0$, we have $p_0 = 0$.

4) The pair of function $(E, E + \tilde{p})$ with $E := A(\psi + p) - \tilde{p}$ forms a mathematical entropy pair for system (41), in that they satisfy the following entropy relation for smooth solution $(A, \bar{u}_\theta, \bar{u}_s)$:

$$\partial_t E + \text{div}_{\theta,s} \left(\begin{pmatrix} \frac{3}{2} \frac{\bar{u}_\theta}{R} \\ \bar{u}_s \end{pmatrix} \left(E + \tilde{p} - \frac{9}{16} A\bar{u}_\theta^{-2} \right) \right) = \frac{9}{4} Rk\bar{u}_\theta^{-2} + kR\bar{u}_s^{-2}.$$

5) The quantity E is consistent with the total energy energy

$e = \frac{\varepsilon^2 u_r^2 + u_\theta^2 + u_s^2}{2}$ of the Navier-Stokes Equations (25)-(28), in the sense that,

$$\begin{aligned} & \partial_t \left(\int_0^R r e \right) + \int_0^R r \text{div}(\mathbf{u}(e + p)) \\ &= \partial_t E + \text{div}_{\theta,s} \left(\begin{pmatrix} \frac{3}{2} \frac{\bar{u}_\theta}{R} \\ \bar{u}_s \end{pmatrix} \left(E + \tilde{p} - \frac{9}{16} A\bar{u}_\theta^{-2} \right) \right) + O(\varepsilon) \end{aligned}$$

where $\mathbf{u} = \begin{pmatrix} \varepsilon u_r \\ u_\theta \\ u_s \end{pmatrix}$.

Remark. The condition $Ap'(A) - \frac{9}{8}\bar{u}_\theta^{-2} \neq 0$ is always satisfied in real life situations [12] [17].

Proof.

1) To prove the hyperbolicity of system (41), we write

$$\partial_t U + H_\theta \partial_\theta U + H_s \partial_s U = S$$

where

$$U = \begin{pmatrix} A \\ Q_{R\theta} \\ Q_s \end{pmatrix}, H_\theta = \begin{pmatrix} -\frac{Q_{R\theta}}{A^2} & \frac{1}{A} & 0 \\ -\frac{Q_{R\theta}^2}{A^3} + Ap'(A) & \frac{Q_{R\theta}}{A^2} & 0 \\ -2\frac{Q_{R\theta}Q_s}{A^3} & \frac{Q_s}{A^2} & \frac{Q_{R\theta}}{A^2} \end{pmatrix},$$

$$H_s = \begin{pmatrix} 0 & 0 & 1 \\ -\frac{Q_{R\theta}Q_s}{A^2} & \frac{Q_s}{A} & \frac{Q_{R\theta}}{A} \\ -\frac{Q_s^2}{A^2} + \frac{Q_{R\theta}^2}{A^3} + Ap'(A) & -\frac{Q_{R\theta}}{A^2} & 2\frac{Q_s}{A} \end{pmatrix}, S = \begin{pmatrix} 0 & & \\ \frac{2R}{3}C \sin \theta \frac{Q_s^2}{A} + 2Rk \frac{Q_{R\theta}}{A} & & \\ -\frac{2R}{3}C \sin \theta \frac{Q_s Q_{R\theta}}{A^2} + kR \frac{Q_s}{A} & & \end{pmatrix}$$

Then, remark that the eigenvalues for H_θ are

$$Sp(H_\theta) = \left\{ \frac{Q_{R\theta}}{A^2}, \sqrt{p'(A)}, -\sqrt{p'(A)} \right\}. \text{ For } H_s, \text{ the eigenvalues are}$$

$$Sp(H_s) = \left\{ \frac{Q_s}{A}, \frac{Q_s}{A} - \sqrt{Ap'(A)}, \frac{Q_s}{A} + \sqrt{Ap'(A)} \right\}. \text{ The system (41) is strictly hyper-$$

bolic if $A > 0$ and $\frac{Q_{R\theta}}{A^2} \neq \pm \sqrt{p'(A)}$ which can be written as

$$Ap'(A) - \frac{9}{8}u_\theta^{-2} \neq 0.$$

2) Next, from simple manipulation, system (41) becomes,

$$\begin{cases} \partial_t A + \partial_\theta \left(\frac{3}{2} A \frac{\bar{u}_\theta}{R} \right) + \partial_s (A \bar{u}_s) = 0, \\ \partial_t \left(\frac{3R}{4} A \bar{u}_\theta \right) + \partial_\theta \left(\frac{9R}{16} \frac{A \bar{u}_\theta^{-2}}{R} \right) + \partial_s \left(\frac{3R}{4} A \bar{u}_\theta \bar{u}_s \right) + A \partial_\theta p = \frac{2R}{3} C \sin \theta A \bar{u}_s^{-2} + \frac{3R}{2} R k \bar{u}_\theta, \\ \partial_t (A \bar{u}_s) + \partial_\theta \left(\frac{3}{2} A \frac{\bar{u}_s \bar{u}_\theta}{R} \right) + \partial_s \left(A \bar{u}_s^{-2} - \frac{9}{16} A \bar{u}_\theta^{-2} \right) + A \partial_s p = -C \sin \theta A \bar{u}_s \bar{u}_\theta + k R \bar{u}_s, \\ p = p_{ext} + b \frac{R - R_0}{R^2}. \end{cases}$$

We first focus on the second equation, dividing by R , we have,

$$\begin{aligned} \partial_t \left(\frac{3}{4} A \bar{u}_\theta \right) + \partial_\theta \left(\frac{9}{16} \frac{A \bar{u}_\theta^{-2}}{R} \right) + \partial_s \left(\frac{3}{4} A \bar{u}_\theta \bar{u}_s \right) + \frac{3}{4R} A \bar{u}_\theta \left[\partial_t R + \frac{3}{4} \frac{\bar{u}_\theta}{R} \partial_\theta R + \bar{u}_s \partial_s R \right] \\ + \frac{R}{2} \partial_\theta p = \frac{2}{3} C \sin \theta A \bar{u}_s^{-2} + \frac{3}{2} R k \bar{u}_\theta. \end{aligned}$$

Then, we use the mass conservation Equation (36) and divide by A to get,

$$\begin{aligned} \partial_t \left(\frac{3}{4} \bar{u}_\theta \right) + \frac{\bar{u}_\theta}{R} \partial_\theta \left(\frac{9}{16} \bar{u}_\theta \right) - \frac{9}{16} \frac{\bar{u}_\theta}{A} \partial_\theta \left(A \frac{\bar{u}_\theta}{R} \right) + \frac{3}{4R} \bar{u}_\theta \left[\partial_t R + \frac{3}{4} \frac{\bar{u}_\theta}{R} \partial_\theta R + \bar{u}_s \partial_s R \right] \\ + \bar{u}_s \partial_s \left(\frac{3}{4} \bar{u}_\theta \right) + \frac{R}{2A} \partial_\theta p = \frac{2}{3} C \sin \theta \bar{u}_s^{-2} + \frac{3}{2A} R k \bar{u}_\theta \end{aligned}$$

which can be easily written as,

$$\partial_i \left(\frac{3}{4} \bar{u}_\theta \right) + \frac{3}{4R} \bar{u}_\theta \left[\partial_i R + \bar{u}_s \partial_s R \right] + u_s \partial_s \left(\frac{3}{4} \bar{u}_\theta \right) + \frac{1}{R} \partial_\theta p = \frac{2}{3} C \sin \theta \bar{u}_s^{-2} + \frac{3}{2A} R k \bar{u}_\theta.$$

Finally, we multiply by $\frac{3}{2} \bar{u}_\theta$ to get,

$$\begin{aligned} & \partial_i \left(\frac{9}{16} \bar{u}_\theta^{-2} \right) + \frac{9}{8R} \bar{u}_\theta^{-2} \left[\partial_i R + \bar{u}_s \partial_s R \right] + u_s \partial_s \left(\frac{9}{16} \bar{u}_\theta^{-2} \right) + \frac{3}{2} \frac{u_\theta}{R} \partial_\theta p \\ & = C \sin \theta \bar{u}_\theta \bar{u}_s^{-2} + \frac{9}{4A} R k \bar{u}_\theta^{-2}. \end{aligned}$$

Similarly, for the third equation in system (41), using the divergence equation and dividing by A leads to,

$$\begin{aligned} & \partial_i (\bar{u}_s) + \frac{3}{2} \frac{\bar{u}_\theta}{R} \partial_\theta (\bar{u}_s) + \bar{u}_s \partial_s (\bar{u}_s) - \frac{1}{A} \partial_s \left(\frac{9}{16} A \bar{u}_\theta^{-2} \right) + \partial_s p \\ & = -C \sin \theta \bar{u}_s \bar{u}_\theta + \frac{1}{A} k R \bar{u}_s, \end{aligned}$$

and multiplying by \bar{u}_s ,

$$\begin{aligned} & \partial_i \left(\frac{\bar{u}_s^{-2}}{2} \right) + \frac{3}{2} \frac{\bar{u}_\theta}{R} \partial_\theta \left(\frac{\bar{u}_s^{-2}}{2} \right) + \bar{u}_s \partial_s \left(\frac{\bar{u}_s^{-2}}{2} \right) - \frac{\bar{u}_s}{A} \partial_s \left(\frac{9}{16} A \bar{u}_\theta^{-2} \right) + \bar{u}_s \partial_s p \\ & = -C \sin \theta \bar{u}_s^{-2} \bar{u}_\theta + \frac{1}{A} k R \bar{u}_s^{-2}. \end{aligned}$$

Finally gathering our two results we obtain,

$$\begin{aligned} & \partial_i \psi + \frac{3}{2} \frac{\bar{u}_\theta}{R} \partial_\theta \left(\psi + p - \frac{9}{16} \bar{u}_\theta^{-2} \right) + \bar{u}_s \partial_s (\psi + p) + \frac{9}{8R} \bar{u}_\theta^{-2} \left[\partial_i R + \bar{u}_s \partial_s R \right] \\ & - \frac{\bar{u}_s}{A} \partial_s \left(\frac{9}{16} A \bar{u}_\theta^{-2} \right) = \frac{9}{4A} R k \bar{u}_\theta^{-2} + \frac{1}{A} k R \bar{u}_s^{-2} \end{aligned}$$

where $\psi = \frac{9}{16} \bar{u}_\theta^{-2} + \frac{1}{2} \bar{u}_s^{-2}$ is the total head. Reminding $\bar{p} = p - \frac{9}{16} \bar{u}_\theta^{-2}$, we get,

$$\partial_i \psi + \frac{3}{2} \frac{\bar{u}_\theta}{R} \partial_\theta (\psi + \bar{p}) + \bar{u}_s \partial_s (\psi + \bar{p}) + \frac{p - \bar{p}}{A} \partial_i A = \frac{9}{4A} R k \bar{u}_\theta^{-2} + \frac{1}{A} k R \bar{u}_s^{-2}.$$

3) The proof is based on simple algebraic computations and is left to the reader.

4) We consider the head Equation (42) and multiply by A ,

$$\begin{aligned} & \partial_i (A\psi) - \psi \partial_i A + \partial_\theta \left(\frac{3}{2} \frac{A \bar{u}_\theta}{R} (\psi + \bar{p}) \right) + \partial_s (A \bar{u}_s (\psi + \bar{p})) + (\psi + \bar{p}) \partial_i A \\ & + (p - \bar{p}) \partial_i A = \frac{9}{4} R k \bar{u}_\theta^{-2} + k R \bar{u}_s^{-2}, \end{aligned}$$

leading to

$$\partial_i (A(\psi + p) - \tilde{p}) + \partial_\theta \left(\frac{3}{2} \frac{A \bar{u}_\theta}{R} (\psi + \bar{p}) \right) + \partial_s (A \bar{u}_s (\psi + \bar{p})) = \frac{9}{4} R k \bar{u}_\theta^{-2} + k R \bar{u}_s^{-2},$$

with \tilde{p} such that, $\tilde{p}'(A) = A p'(A)$. We call energy the quantity

$E := A(\psi + p) - \tilde{p}$ and remark,

$$\partial_t(E) + \partial_\theta \left(\frac{3 \bar{u}_\theta}{2 R} \left(E + \tilde{p} - \frac{9}{16} A \bar{u}_\theta^{-2} \right) \right) + \partial_s \left(\bar{u}_s \left(E + \tilde{p} - \frac{9}{16} A \bar{u}_\theta^{-2} \right) \right) = \frac{9}{4} R k \bar{u}_\theta^{-2} + k R \bar{u}_s^{-2}.$$

Moreover, the total energy in our domain $\int_{-\pi}^{\pi} \int_0^L E ds d\theta$ decreases, i.e.

$$\frac{d}{dt}(E_{tot}) = \frac{9}{4} (Rk) \|\bar{u}_\theta\|^2 + (Rk) \|u_s\|^2 \leq 0,$$

with k supposed negative in the domain.

5) In this proof, we use Equations (25)-(28) by omitting $\tilde{\tau}$ and gathering all remainder terms in $O(\varepsilon)$. Multiplying respectively the radial momentum Equation (26), angular momentum Equation (27), and axial momentum Equation (28) by u_r , u_θ , and u_s , and summing up the three equations obtained, one has

$$\begin{aligned} & \partial_t \left(\frac{u_\theta^2 + u_s^2}{2} \right) + u_r \partial_r \left(\frac{u_\theta^2 + u_s^2}{2} \right) + \frac{u_\theta}{r} \partial_\theta \left(\frac{u_\theta^2 + u_s^2}{2} \right) + u_s \partial_s \left(\frac{u_\theta^2 + u_s^2}{2} \right) \\ & + u_r \partial_r p + \frac{u_\theta}{r} \partial_\theta p + u_s \partial_s p \\ & = \frac{V_0}{\varepsilon} \left[\frac{u_s}{r \beta} \partial_r (r \beta \partial_r u_s) + \varepsilon \frac{\mathcal{C} \cos \theta}{r} u_s^2 + \frac{u_\theta}{r \beta} \partial_r \left(r \beta \left(\partial_r u_\theta - \frac{u_\theta}{r} \right) \right) \right. \\ & \left. + u_\theta \frac{\partial_r u_\theta}{r} - \frac{u_\theta^2}{r^2} \right] + O(\varepsilon). \end{aligned}$$

Defining $\phi = \frac{u_\theta^2 + u_s^2}{2}$, recalling $e = \frac{\varepsilon^2 u_r^2 + u_\theta^2 + u_s^2}{2}$, and therefore $e = \phi + O(\varepsilon^2)$, keeping it in mind, multiplying by $r \beta$ the previous equation, we have:

$$\begin{aligned} & \partial_t (r \phi) + \partial_r (r u_r (\phi + p)) + \partial_\theta (u_\theta (\phi + p)) + \partial_s (r u_s (\phi + p)) \\ & = \frac{V_0}{\varepsilon} \left[u_s \partial_r (r \beta \partial_r u_s) + \varepsilon \mathcal{C} \cos \theta u_s^2 + \frac{u_\theta}{r} \partial_r \left(r^2 \beta \left(\partial_r u_\theta - \frac{u_\theta}{r} \right) \right) \right] + O(\varepsilon). \end{aligned}$$

We proceed by integrating the above-equation, making use of the normal boundary condition from Equation (29), to get:

$$\begin{aligned} & \partial_t (A \bar{\phi}) + \partial_\theta \left(\int_0^R u_\theta (\phi + p) \right) + \partial_s \left(\int_0^R r u_s (\phi + p) \right) + \partial_r A p (r = R) \\ & = \frac{V_0}{\varepsilon} \int_0^R \left[u_s \partial_r (r \beta \partial_r u_s) + \varepsilon \mathcal{C} \cos \theta u_s^2 + \frac{u_\theta}{r} \partial_r \left(r^2 \beta \left(\partial_r u_\theta - \frac{u_\theta}{r} \right) \right) \right] + O(\varepsilon), \end{aligned}$$

where $\bar{\phi} = \frac{1}{A} \int_0^R r \phi$. Using the profile from Equations (35) and (34) we get,

$$\begin{aligned} & \partial_t (A (\bar{\phi} + p(r = R)) - \tilde{p}) + \partial_\theta \left(\frac{3 \bar{u}_\theta}{2 R} A (\bar{\phi} + \bar{p}) \right) + \partial_s (\bar{u}_s A (\bar{\phi} + \bar{p})) \\ & = \frac{V_0}{\varepsilon} \left[\bar{u}_s R \beta (r = R) (\partial_r u_s)(r = R) + \varepsilon \mathcal{C} \cos \theta R \bar{u}_s^{-2} \right. \\ & \left. + \frac{3 \bar{u}_\theta}{2 R} \left(R^2 \beta (r = R) \left((\partial_r u_\theta)(r = R) - \frac{u_\theta(r = R)}{R} \right) \right) \right] + O(\varepsilon), \end{aligned}$$

where \tilde{p} is such that, $\tilde{p}'(A) = A p'_R(A)$ with $p_R = p(r = R)$. Finally, using

the boundary condition Equations (31) and (30) in the preceding equation, we get:

$$\begin{aligned} & \partial_t \left(A(\bar{\phi} + p(r=R)) - \tilde{p} \right) + \partial_\theta \left(\frac{3 \bar{u}_\theta}{2 R} A(\bar{\phi} + \bar{p}) \right) + \partial_s \left(\bar{u}_s A(\bar{\phi} + \bar{p}) \right) \\ &= \frac{v_0}{\varepsilon} \left[\bar{u}_s R \left(\frac{\varepsilon}{v_0} k \bar{u}_s - \varepsilon C \cos \theta \bar{u}_s \right) + \varepsilon C \cos \theta R \bar{u}_s^{-2} + \frac{9}{4} \bar{u}_\theta R \frac{\varepsilon}{v_0} k \bar{u}_\theta \right] + O(\varepsilon), \end{aligned}$$

yielding to

$$\begin{aligned} & \partial_t \left(A(\bar{\phi} + p(r=R)) - \tilde{p} \right) + \partial_\theta \left(\frac{3 A \bar{u}_\theta}{2 R} (\bar{\phi} + \bar{p}) \right) + \partial_s \left(A \bar{u}_s (\bar{\phi} + \bar{p}) \right) \\ &= R k \bar{u}_s^{-2} + \frac{9}{4} R k \bar{u}_\theta^{-2} + O(\varepsilon). \end{aligned}$$

Remarking that $\bar{\phi} = \frac{1}{A} \int_0^R r \frac{u_\theta^2 + u_s^2}{2} dr = \psi$, we obtain the result:

$$\begin{aligned} & \partial_t \left(\int_0^R r e \right) + \int_0^R r \operatorname{div}(\mathbf{u}(e+p)) \\ &= \partial_t E + \operatorname{div}_{\theta,s} \left(\begin{pmatrix} \frac{3 \bar{u}_\theta}{2 R} \\ \bar{u}_s \end{pmatrix} \left(E + \tilde{p} - \frac{9}{16} A \bar{u}_\theta^{-2} \right) \right) + O(\varepsilon). \end{aligned}$$

□

3. A Discontinuous Galerkin Method for the Two-Dimensional Model

In this section, we present a discontinuous Galerkin method to solve a general two-dimensional hyperbolic system of equations, in particular for model (41), using the RKDG method from [18] on a cartesian grid. It can be easily generalized to non-conforming meshes (see for instance [20] [21]).

3.1. Model Problem

Our aim is to construct a high-order numerical method for the blood flow problem from Equation (41) derived in Section 2. To this purpose, we propose a Discontinuous Galerkin approach for two-dimensional hyperbolic problems following [18]. Let us consider the following non-linear two-dimensional hyperbolic problem:

$$\begin{cases} \partial_t u + \partial_x f_1 + \partial_y f_2 = s, & \forall (t, x, y) \in]0, T] \times]a_1, b_1[\times]a_2, b_2[, \\ u(t=0, x, y) = u_0(x, y), & \forall (x, y) \in [a_1, b_1] \times [a_2, b_2], \\ u(t, x = a_1, y) = u_{\text{left}}(t, y), & \forall (t, y) \in]0, T] \times [a_2, b_2[, \\ u(t, x = b_1, y) = u_{\text{right}}(t, y), & \forall (t, y) \in]0, T] \times [a_2, b_2[, \\ u(t, x, y = a_2) = u_{\text{bottom}}(t, x), & \forall (t, x) \in]0, T] \times [a_1, b_1[, \\ u(t, x, y = b_2) = u_{\text{top}}(t, x), & \forall (t, x) \in]0, T] \times [a_1, b_1[. \end{cases} \tag{43}$$

where $(u_{\text{right}}, u_{\text{left}}, u_{\text{top}}, u_{\text{bottom}}) \in (\mathbb{R}^d)^4$ are Dirichlet boundary conditions and

$u_0(x, y) \in \mathbb{R}^d$ is the initial condition. Here $f_1(t, x, y, u) \in \mathbb{R}^d$ is the advection component in the x direction, $f_2(t, x, y, u)$ is the advection component in the y direction, and $s(t, x, y, u, \nabla_{x,y}u)$ is the source term.

3.2. Space Discretization

Since the objective is to solve Equation (43) using a numerical scheme, defining a partition of the computational domain $[a_1, b_1] \times [a_2, b_2]$ is mandatory. For simplicity, a cartesian fixed mesh is used and its description is given in subsection 3.2.1. Following this description, we derive the discrete variational formulation in subsection 3.2.2. Finally, this will lead to an ODE system in subsection 3.2.3.

3.2.1. Mesh Description

Let us define \mathcal{E} a partition of the computational domain $[a_1, b_1] \times [a_2, b_2]$. The set of all open faces of all elements $E \in \mathcal{E}$ is denoted by \mathcal{F} . Moreover, we can define two subsets of \mathcal{F} , \mathcal{F}^∂ for the boundary faces and \mathcal{F}^{in} for the interior faces.

For a given element $E \in \mathcal{E}$, there exists a set of face $\mathcal{F}^E = \{F \in \mathcal{F} \mid F \in \partial E\}$ which defines boundaries of E . Then, for all interior faces of E , i.e. $\forall F \in \mathcal{F}^E \cap \mathcal{F}^{\text{in}}$, there exists a neighboring element E_r such that $E \cap E_r = F$.

Consequently, the normal unit vector $\mathbf{n}_{E,F} := \begin{pmatrix} n_x \\ n_y \end{pmatrix}$ pointing from E to E_r is well defined. Moreover for all boundary faces of E , i.e., $\forall F \in \mathcal{F}^E \cap \mathcal{F}^\partial$, there exists E_∂ a fictitious element such that $E \cap E_\partial = F$. Again, $\mathbf{n}_{E,F}$ is well defined.

For simplicity, all elements are considered rectangular and faces are straight lines with normal vector $\mathbf{n}_{E,F} = \begin{pmatrix} \pm 1 \\ 0 \end{pmatrix}$ for vertical faces or $\mathbf{n}_{E,F} = \begin{pmatrix} 0 \\ \pm 1 \end{pmatrix}$ for horizontal ones.

In the discontinuous Galerkin framework, the solutions are considered piecewise polynomials per element. Many basis exist for the polynomial space over an element as monomial, Legendre, Dubiner, and others [20] [22]. For simplicity, we only consider the monomial basis in this section. Finally, the approximate space is given as

$$V_p(\mathcal{E}) = \{v : [a_1, b_1] \times [a_2, b_2] \rightarrow \mathbb{R}; v|_E \in \mathbb{P}^p(E), \forall E \in \mathcal{E}\}.$$

3.2.2. Weak Formulation

By multiplying the system (43) by a test function $v \in V_p(\mathcal{E})$ and integrating over an element E , we obtain

$$\int_E \partial_t uv - \int_E (f_1 \partial_x v + f_2 \partial_y v) dE + \sum_{F \in \mathcal{F}^E} \int_F \begin{pmatrix} f_1 \\ f_2 \end{pmatrix} \cdot \mathbf{n}_{E,F} v|_E dF = \int_E s v dE.$$

We look for $u_{DG} \in V_p(\mathcal{E})$ such that

$$\int_E \partial_t u_{DG} v - \int_E (f_1 \partial_x v + f_2 \partial_y v) dE + \sum_{F \in \mathcal{F}^E} \int_F \hat{f} v|_E dF = \int_E s v dE. \tag{44}$$

where \hat{f} is the numerical flux which we choose, for simplicity, as the Rusanov flux

$$\hat{f}(t, x, y, u_{DG}, \mathbf{n}_{E,F}) = \left\{ \begin{pmatrix} f_1(t, x, y, u_{DG}) \\ f_2(t, x, y, u_{DG}) \end{pmatrix} \cdot \mathbf{n}_{E,F} \right\} + \frac{c}{2} [u_{DG}],$$

where $c = \max_{i=1, \dots, d} |\lambda_i(t, x_n, u, \mathbf{n})|$ with λ_i the eigenvalues of $\begin{pmatrix} \nabla_u f_1 \\ \nabla_u f_2 \end{pmatrix} \cdot \mathbf{n}$,

$\{v\} = \frac{v|_E + v|_{E_r}}{2}$ the average of v at the face F and $[v] = v|_E - v|_{E_r}$ the jump of

v across the face F . Remark that, for a face $F \in F^\partial$, we consider

$u_{DG}|_{E^\partial}(F) = u_{\text{boundary}}$ where u_{boundary} are the boundary conditions set in Equation (43).

3.2.3. ODE System

Consider the monomial two-dimensional basis functions of $\mathbb{P}_p(E)$ defined as

$abc = \frac{(p+1)(p+2)}{2}$ function defined by,

$$\varphi_i^E(x, y) = \varphi_{\frac{k(k+1)}{2} + j}^E(\hat{x}, \hat{y}) = \hat{x}^{k-j} \hat{y}^j, \tag{45}$$

where $0 \leq k \leq p$, $0 \leq j \leq k$ and, $\hat{x} = \frac{2}{h_x} \left(x - x_{n+\frac{1}{2}} \right)$, $\hat{y} = \frac{2}{h_y} \left(y - y_{n+\frac{1}{2}} \right)$, with

h_x and h_y the length and the width of the element E respectively. We look

for a solution u_{DG} of Equation (44) in $V_p(\mathcal{E})$ that we decompose in the basis Equation (45):

$$u_{DG}(t, x, y) = \sum_{E \in \mathcal{E}} \sum_{i=0}^{abc} \varphi_i^E(x, y) U_i^E(t) \mathbb{1}_E(x, y),$$

where the coefficients $U_i^E(t)$ are unknown time-dependent functions and

$\mathbb{1}_E(x, y)$ is the characteristic function of the element E . Similarly,

$v(x, y) = \sum_{E \in \mathcal{E}} \sum_{i=0}^{abc} \varphi_i^E(x, y) V_i^E \mathbb{1}_E(x, y)$, with V_i^E constant coefficients. Fol-

lowing these definitions, one can write:

$$\begin{aligned} & \sum_{E \in \mathcal{E}} \sum_{i=0}^{abc} \sum_{j=0}^{abc} \left(\int_E \phi_i^E \phi_j^E \right) \partial_t U_i^E V_j^E - \sum_{E \in \mathcal{E}} \sum_{j=0}^{abc} \int_E (f_1 \partial_x \phi_j^E + f_2 \partial_y \phi_j^E) dE V_j^E \\ & + \sum_{E \in \mathcal{E}} \sum_{j=0}^{abc} \sum_{F \in \mathcal{F}^E} \int_F \hat{f} \phi_j^E dF V_j^E = \sum_{E \in \mathcal{E}} \sum_{j=0}^{abc} \int_E s \phi_j^E dE V_j^E. \end{aligned}$$

Finally, this can be written in matrix form as,

$$V^t M \partial_t U - V^t F(t, U) = V^t S(t, U),$$

where, $U = (U_i^E)_{i \in \llbracket 1, abc \rrbracket, E \in \mathcal{E}}$, $V = (V_i^E)_{i \in \llbracket 1, abc \rrbracket, E \in \mathcal{E}}$,

$M = \left(\int_E \phi_i^E \phi_j^E \right)_{i \in \llbracket 1, abc \rrbracket, j \in \llbracket 1, abc \rrbracket, E \in \mathcal{E}}$ and

$F(t, U) = \left(\int_E (f_1 \partial_x \phi_j^E + f_2 \partial_y \phi_j^E) dE - \sum_{F \in \mathcal{F}^E} \int_F \hat{f} \phi_j^E dF \right)_{j \in \llbracket 1, abc \rrbracket, E \in \mathcal{E}}$,

$S(t, U) = \left(\int_E s \phi_j^E dE \right)_{j \in \llbracket 1, nbc \rrbracket, E \in \mathcal{E}}$. Simplifying by V' , we get the following ODE system

$$M \partial_t U = F(t, U) + S(t, U). \tag{46}$$

3.3. Time Discretization

In this section, we propose a time discretization based on the Runge-Kutta (RK) methods applied to the ODE system (46).

3.3.1. RK Methods

We recall the RK methods presented in [23]. RK methods are used to solve a system of ODEs of the form

$$U'(t) = R(t, U) \tag{47}$$

where R is some function. Let $t_k \in [0, T]$ and Δt a well-chosen time step, s -stage-Runge-Kutta methods reads, for $i \in \llbracket 1, s \rrbracket$,

$$\begin{cases} K^{(i)} = U^{(k)} + \Delta t \sum_{j=1}^s a_{ij} R(t_k + c_j \Delta t, K^{(j)}), \\ U^{(k+1)} = U^{(k)} + \Delta t \sum_{i=1}^s b_i R(t_k + c_i \Delta t, K^{(i)}), \end{cases}$$

where $U^{(k)} \approx U(t_k)$ is the approximate solution of Equation (47) at time t_k and $U^{(k+1)} \approx U(t_k + \Delta t)$ the approximate solution at time $t_{k+1} = t_k + \Delta t$. The Butcher coefficient $(a_{ij})_{i \in \llbracket 1, s \rrbracket, j \in \llbracket 1, s \rrbracket}$, $(b_i)_{i \in \llbracket 1, s \rrbracket}$, $(c_i)_{i \in \llbracket 1, s \rrbracket}$ are constrained, at a minimum, by certain order of accuracy and stability considerations as discussed in [23].

3.3.2. Application to the ODE System

We write the ODE from Equation (46) in the form of Equation (47) leading to, $\partial_t(U) = M^{-1}R(t, U)$ with $R(t, U) = F(t, U) + S(t, U)$ leading to the following scheme

$$\begin{cases} MK^{(i)} = MU^{(k)} + \Delta t \sum_{j=1}^s a_{ij} R(t_k + c_j \Delta t, K^{(j)}), \\ MU^{(k+1)} = MU^{(k)} + \Delta t \sum_{i=1}^s b_i R(t_k + c_i \Delta t, K^{(i)}), \end{cases} \tag{48}$$

The time step is given by

$$\Delta t = \frac{\text{cfl}}{2p+1} \min_{E \in \mathcal{E}} \frac{\text{Area}(E)}{\text{Diam}(E)} \frac{1}{c^k},$$

where $\text{cfl} \in]0, 1]$, p is the polynomial degree, $\text{Area}(E)$, the area of an element, $\text{Diam}(E)$ its diameter and c^k , the characteristic speed define as

$c^k = \max_{E \in \mathcal{E}} \left| \lambda(t_k, U^k, E) \right|$, with $\lambda(t, u, E)$ the maximum of the eigenvalues of $\nabla_u f_1(t, x, y, u) + \nabla_u f_2(t, x, y, u)$ for $(x, y) \in E$. This CFL condition is obtained by a von Neumann stability analysis of the RKDG methods [18] [24].

We use the following explicit time scheme depending on p (see **Table 1**), and

butcher tables can be found in [21] [25]. Those algorithms are sometimes called the TVD-RK (Total Variation Diminishing-RK) scheme or SSP-RK (Strong Stability Preserving-RK) scheme.

Table 1. Time schemes for different values of p .

p	Time scheme
0	Euler
1	TVDRK2
2	TVDRK3
3	TVDRK4
4	TVDRK5

3.4. Still-Steady States Solutions

One can easily obtain a well-balanced scheme for the two-dimensional blood flow problem in Equation (41) derived in Section 2 by a simple change of variable. This is an important stability property of the numerical scheme. It is achieved by introducing the change of variable

$$a = A - A_0.$$

Thus, one can write the system (41) as

$$\begin{cases} \partial_t (a) + \partial_\theta \left(\frac{Q_{R\theta}}{a + A_0} \right) + \partial_s (Q_s) = 0, \\ \partial_t (Q_{R\theta}) + \partial_\theta \left(\frac{Q_{R\theta}^2}{2(a + A_0)^2} + (a + A_0) p \right) + \partial_s \left(\frac{Q_{R\theta} Q_s}{a + A_0} \right) \\ = \frac{2R}{3} C \sin \theta \frac{Q_s^2}{a + A_0} + 2Rk \frac{Q_{R\theta}}{a + A_0} + \partial_\theta (a + A_0) p, \\ \partial_t (Q_s) + \partial_\theta \left(\frac{Q_s Q_{R\theta}}{(a + A_0)^2} \right) + \partial_s \left(\frac{Q_s^2}{a + A_0} - \frac{Q_{R\theta}^2}{2(a + A_0)^2} + (a + A_0) p \right) \\ = -\frac{2R}{3} C \sin \theta \frac{Q_s Q_{R\theta}}{(a + A_0)^2} + kR \frac{Q_s}{a + A_0} + \partial_s (a + A_0) p, \\ p = p_{ext} + b \frac{R - R_0}{R_0^2}. \end{cases} \tag{49}$$

Then, we have the following property:

Proposition 2. The numerical scheme in Equation (48) preserves exactly the still-steady states solutions (see Theorem 1).

The proof is based on the recursivity principle and is left to the reader.

4. Test Cases

In this chapter, we present several test cases for the Discontinuous Galerkin (DG) method developed in Section 3 for the two-dimensional blood flow system (41). The main objective of these test cases is to evaluate the robustness of the DG

method. From now on, we consider the model (49) instead of Equation (41).

4.1. Convergence Order

To solve the two-dimensional blood flow model (see Section 2), we use the DG method presented in Section 3. We aim to compute the numerical order of convergence for a given exact solution. We consider the following friction coefficient

$$k = -11 \frac{\nu}{R}. \text{ We also recall the pressure } p = b \frac{\sqrt{A} - \sqrt{A_0}}{A_0} \text{ with } \beta \text{ a physical parameter for the wall. The physical and numerical parameters used are given in Table 2 together with the following geometric parameters:}$$

$$\mathbf{c}(s) = \frac{(\cos(s), \sin(s), s)}{\sqrt{2}}, \text{ leading to, } \mathbf{t}(s) = \frac{(-\sin(s), \cos(s), 1)}{\sqrt{2}}, \text{ and,}$$

$\mathbf{n}(s) = (-\cos(s), -\sin(s), 0)$ where $\mathcal{C}(s) = \sqrt{2}$. We compute a reference solution for the 2D numerical scheme, as shown in Figure 3, using 128×128

elements. In Figure 4, we compute the convergence order for $N \times N$ elements with $N = 4, 8, 16$. We compute the error $\epsilon = \|u_{REF} - u_{DG}\|_{L^2([0,1])}$ with u_{REF} the reference solution calculated before and u_{DG} the solution obtain at time $t = T$. We show that all variables converge at an order of $p + 1$ in agreement with the classical result in the literature on the RKDG schemes (see for instance [18]).

Table 2. Parameters for the convergence test.

Parameter	Value
β	3
A_0	2
ν	3×10^{-2}
T	1
L	10
cfl	0.5

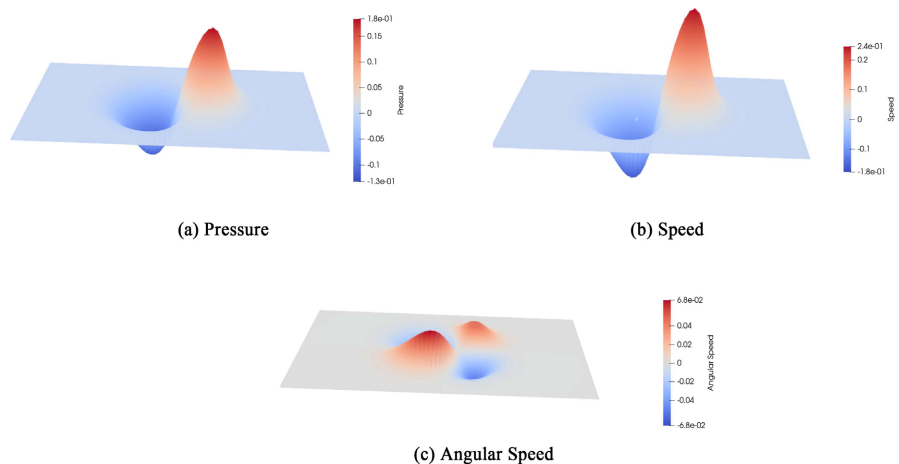


Figure 3. Reference solution for the 2D numerical scheme.

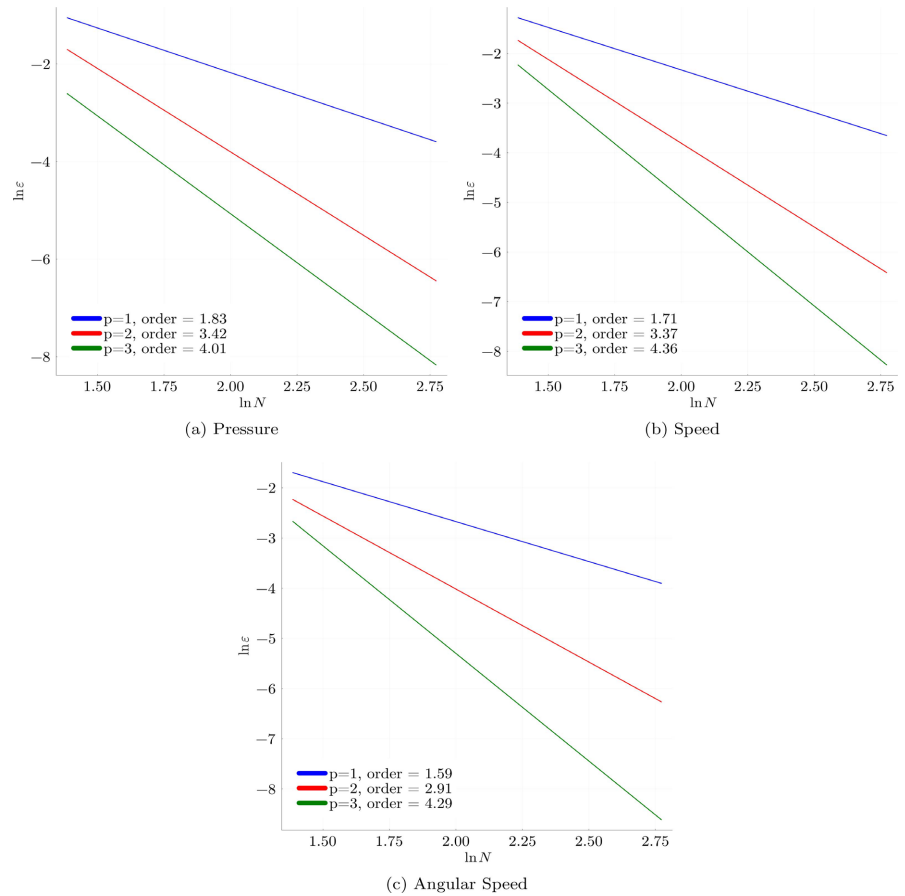


Figure 4. Convergence order for the 2D numerical scheme.

4.2. Stationary Solutions

For this test case, the aim is to show that the numerical method captures exactly the still-steady state solutions. We have used the following parameters in **Table 3** and the following geometrical parameters:

$$c(s) = \left(s, e^{-\frac{1}{2}\left(s-\frac{L}{2}\right)^2}, 0 \right), \text{ leading to, } t(s) = \frac{\left(1, -\left(s-\frac{L}{2}\right) e^{-\frac{1}{2}\left(s-\frac{L}{2}\right)^2}, 0 \right)}{\sqrt{1 + \left(s-\frac{L}{2}\right)^2 e^{-\left(s-\frac{L}{2}\right)^2}}}, \text{ and,}$$

$$n(s) = \frac{\left(0, \left(\left(s-\frac{L}{2}\right)^2 - 1 \right) e^{-\frac{1}{2}\left(s-\frac{L}{2}\right)^2}, 0 \right)}{\left| \left(s-\frac{L}{2}\right)^2 - 1 \right| e^{-\frac{1}{2}\left(s-\frac{L}{2}\right)^2}} = \left(0, \text{sign} \left(\left(s-\frac{L}{2}\right)^2 - 1 \right), 0 \right),$$

where $C(s) = \frac{\|c''(s)\|}{\|c'(s)\|} = \frac{\left| \left(s-\frac{L}{2}\right)^2 - 1 \right| e^{-\frac{1}{2}\left(s-\frac{L}{2}\right)^2}}{\sqrt{1 + \left(s-\frac{L}{2}\right)^2 e^{-\left(s-\frac{L}{2}\right)^2}}}$. The initial geometry is repre-

sented in **Figure 5** and it is defined by $A_0(x, \theta) = \frac{1}{2} \left(R_0 + (R_1 - R_0) e^{-4 \left(\frac{x-L}{2} \right)^{-2(\theta-\pi)}} \right)^2$.

and characterized by $\beta(x, \theta) = \left(E_0 + (E_1 - E_0) e^{-4 \left(\frac{x-L}{2} \right)^{-2(\theta-\pi)}} \right) \frac{h\sqrt{2}}{2\rho(1-\xi^2)}$. Start-

ing with a null speed, $A = A_0$, as in proved in Theorem 1, in **Figure 6**, we show that the still-steady state's solutions are exactly preserved.

Table 3. Physical and Numerical parameters for the 2D stationary test case.

Parameter	Value	Unit	Description
E_0	3×10^6	$\text{kg}\cdot\text{cm}^{-1}\cdot\text{s}^{-2}$	Minimum Young modulus
E_1	3×10^8	$\text{kg}\cdot\text{cm}^{-1}\cdot\text{s}^{-2}$	Maximum Young modulus
h	0.05	cm	Thickness
ρ	1	$\text{kg}\cdot\text{cm}^{-3}$	Density
ξ	0.0		Poisson coefficient
R_0	0.5	cm	Maximum radius
R_1	0.3	cm	Minimum radius
ν	0.03	$\text{Cm}^2\cdot\text{s}^{-1}$	Kinematic viscosity
T	0.25	s	Final time
L	15	cm	Artery's length
cfl	0.5		Cfl
N_s	32		Number of elements in the s direction
N_θ	32		Number of elements in the θ direction
p	1		Polynomial degree

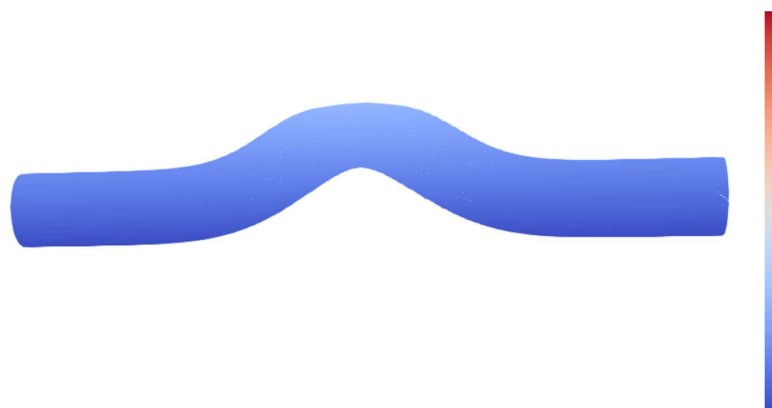


Figure 5. Artery geometry.

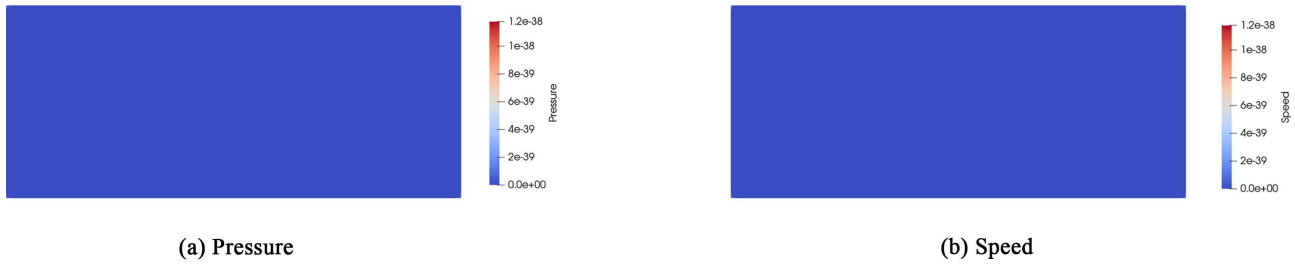


Figure 6. Stationary solutions at $t = T$.

4.3. Realistic Pressure Wave in a Straight Artery

In this test case, we compare the one-dimensional models 1D inviscid from Equation (3) (solved by a TGS-Taylor Galerkin Scheme, see [6]), 1D viscous from Equation (4) (solved by a DG method, see [26]), and 2D Equation (41) solved by the DG method presented in Section 3.

In Table 4, we give the physical and numerical parameters of the test case, also, we consider, for simplicity, the pressure at $r = R$ to be $P = \beta \frac{\sqrt{A} - \sqrt{A_0}}{A_0}$ even in the viscous case in Equation (4). The following parameters are considered:

$$\beta = \frac{Eh\sqrt{\pi}}{\rho(1-\xi^2)}, \quad A_0 = \pi R_0^2$$

In the 2D case, these parameters are:

$$\beta = \frac{Eh}{\sqrt{2}\rho(1-\xi^2)}, \quad A_0 = \frac{R_0^2}{2}$$

We use the following curve $c(s) = (s, 0, 0)$ and we choose $\mathbf{n} = (0, 1, 0)$ by setting the curvature $\mathcal{C}(s) = 0$. To simulate a pressure wave entering into the domain, we use the following sinus-wave:

$$P(0, t) = \begin{cases} P_0 \sin\left(\pi \frac{t}{T_p}\right) & \text{if } t \leq T_p \\ 0 & \text{otherwise} \end{cases}$$

This lead to the following initial and boundary conditions,

$$\begin{aligned} A(s, 0) &= A_0 & Q(s, 0) &= 0 \\ A(0, t) &= \left(\frac{A_0}{\beta} P(0, t) + \sqrt{A_0}\right)^2 & \partial_s Q(0, t) &= 0 \\ \partial_s A(15, t) &= 0 & \partial_s Q(15, t) &= 0 \end{aligned}$$

Table 4. Physical and numerical parameters for TC1 (Realistic Pressure Wave in a straight artery).

Parameter	Value	Unit	Description
E	3×10^6	$\text{kg}\cdot\text{cm}^{-1}\cdot\text{s}^{-2}$	Young modulus
h	0.05	cm	Thickness
ρ	1	$\text{kg}\cdot\text{cm}^{-3}$	Density
ξ	0.0		Poisson coefficient
R_0	0.5	cm	Initial radius

Continued

ν	0 or 0.03	$\text{cm}^2\cdot\text{s}^{-1}$	Kinematic viscosity
T	0.25	s	Final time
L	15	cm	Artery's length
P_0	2×10^4	$\text{kg}\cdot\text{cm}^{-1}\cdot\text{s}^{-2}$	Entering pressure amplitude
T_p	0.165	s	Pressure wave duration
σ	100		penalty parameter
cfl	0.5		Cfl
N	128		Number of elements for the 1D model
N_s	128		Number of elements in the s direction
N_θ	4		Number of elements in the θ direction
p	2		Polynomial degree

and for the 2D, with $P(0, \theta, t) = \begin{cases} P_0 & \text{if } t \leq T_p \\ 0 & \text{otherwise} \end{cases}$, we set

$$\begin{aligned}
 A(s, \theta, 0) &= A_0 & Q_\theta(s, \theta, 0) &= 0 & Q_s(s, \theta, 0) &= 0 \\
 A(0, \theta, t) &= \left(\frac{A_0}{\beta} P(0, \theta, t) + \sqrt{A_0} \right)^2 & \partial_s Q_\theta(0, \theta, t) &= 0 & \partial_s Q_s(0, \theta, t) &= 0 \\
 \partial_s A(15, \theta, t) &= 0 & \partial_s Q_\theta(15, \theta, t) &= 0 & \partial_s Q_s(15, \theta, t) &= 0.
 \end{aligned}$$

Periodic conditions are imposed on the direction θ . **Figure 7** shows the geometry colored with the axial speed at time $t = \frac{T}{2}$. In **Figure 8**, we compare the pressure obtained using the nonviscous 1D model in Equation (3) with the data obtained from [6]. We also display the axial speed of the blood. We do the same in the viscous case (see Equations (4)) in **Figure 9** and in the 2D case (see Equations (41)) in **Figure 10**. Our numerical results are compared to those in [6] where the TGS (Taylor Galerkin Scheme) is used. As expected, our numerical results (2D and 1D) are in a perfect agreement with those obtained in [6]. The results of the 1D and 2D models are almost identical because of the axisymmetry and curvaturless of the geometry. One can also remark that, in this case, the angular speed of the 2D model is almost zero everywhere (at least zero numerically) as shown in **Figure 11**. Moreover, one can see throughout this test case that the 1D viscous models provide mildly different numerical solutions compared to the inviscid models (TGS model and our 1D inviscid model).

4.4. Addon of the 2D Model and the Limit of 1D Model in the Case of Aneurysm

In this test case, we compare the one-dimensional models 1D inviscid from Equation (3) and 2D Equation (41) solved by the DG method presented in Section 3 in the case of a mild and a severe aneurysm to show the addon of the 2D model

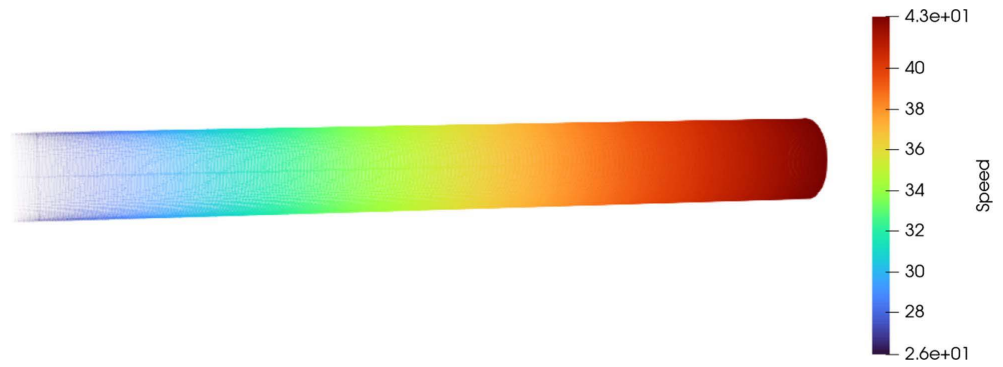


Figure 7. Artery geometry colored with axial speed at time $t = \frac{T}{2}$.

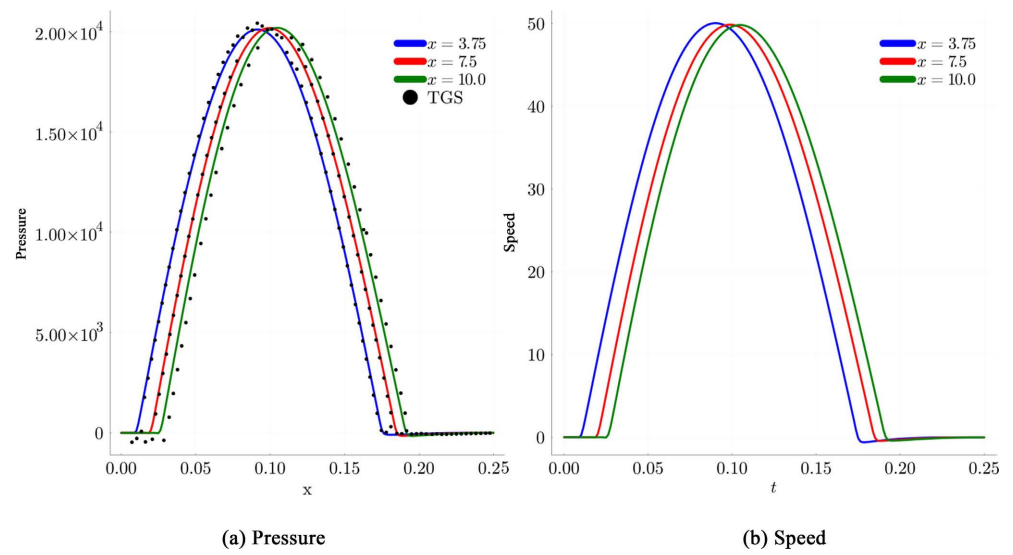


Figure 8. Pressure and Speed for the 1D non-viscous model and comparison with data obtained from [6].

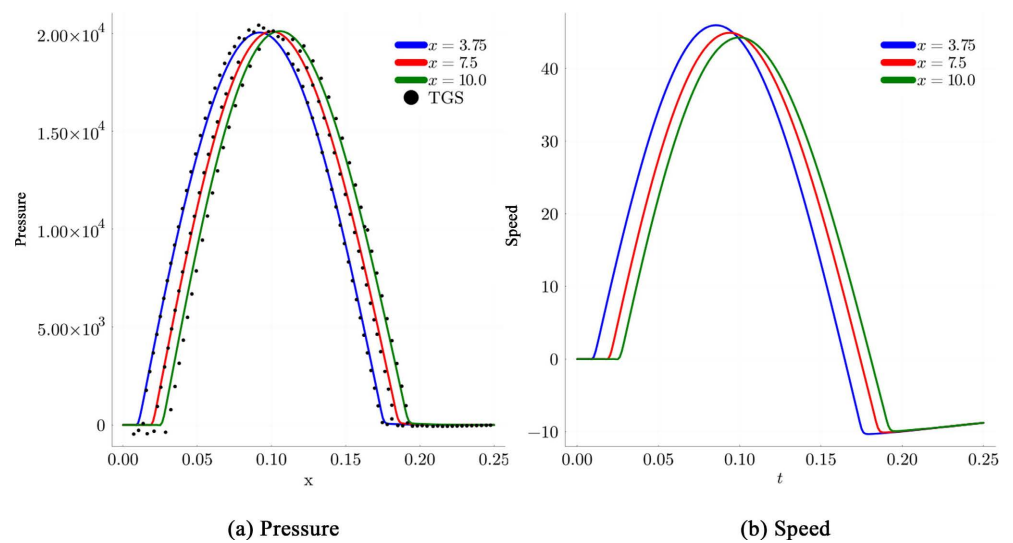


Figure 9. Pressure and Speed for the 1D viscous model and comparison with data obtained from [6].

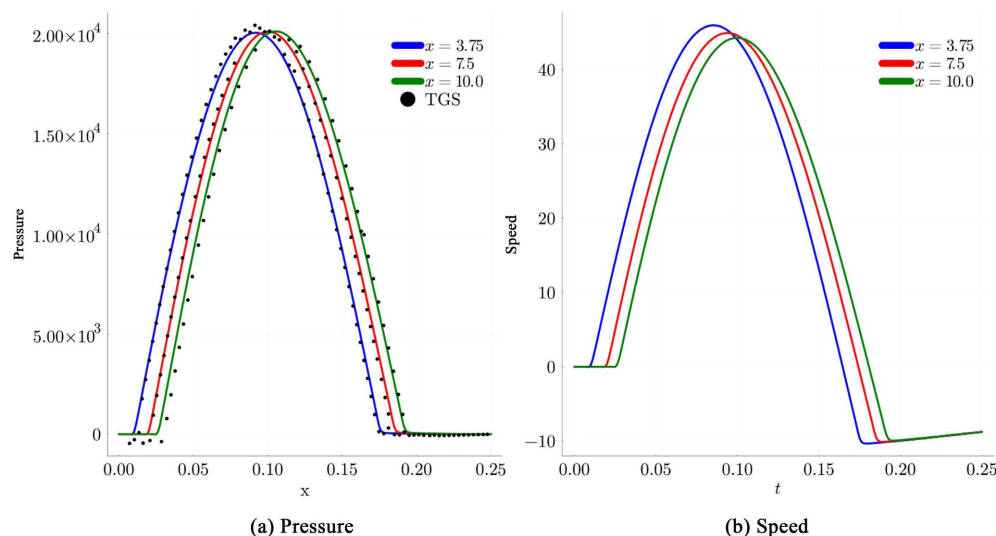


Figure 10. Pressure and Speed for the 2D model and comparison with data obtained from [6].

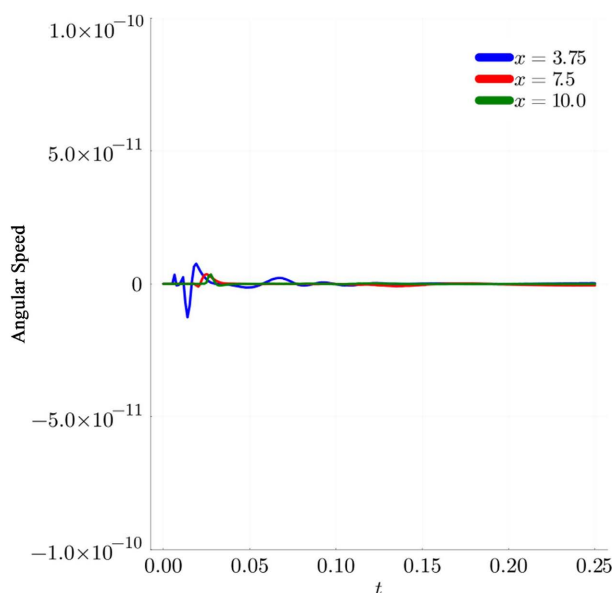


Figure 11. Angular Speed for the 2D model.

and the limit of the 1D model. In the medical literature [27], the classification of aneurysm severity depends on the location. For intracranial aneurysms, diameters below 7 mm are usually considered small, 7 - 12 mm medium, 13 - 24 mm large, and above 25 mm giant. For abdominal aortic aneurysms (AAA), diameters above 5.5 cm are typically considered severe and represent a threshold for surgical intervention.

In Table 5, we present the physical and numerical parameters of the test case. We consider, for simplicity, the pressure at $r = R$ to be $P = \beta \frac{\sqrt{A} - \sqrt{A_0}}{A_0}$.

We consider two different geometries mimicking a mild and a severe aneurysm. The initial geometry is given by:

Table 5. Physical and numerical parameters for TC4 (Addon of the 2D model over the 1D model in complex geometry).

Parameter	Value	Unit	Description
E	3×10^6	$\text{kg}\cdot\text{cm}^{-1}\cdot\text{s}^{-2}$	Young modulus
h	0.1	cm	Thickness
ρ	1	$\text{kg}\cdot\text{cm}^{-3}$	Density
ξ	0.0		Poisson coefficient
R_0	0.5	cm	Initial radius
R_1	2.0	cm	Secondary radius
ν	0 or 0.03	$\text{cm}^2\cdot\text{s}^{-1}$	Kinematic viscosity
T	0.03	s	Final time
L	10	cm	Artery's length
P_0	13,332	$\text{kg}\cdot\text{cm}^{-1}\cdot\text{s}^{-2}$	Entering pressure amplitude
T_p	0.005	s	Pressure wave duration
σ	1		Penalty parameter
cfl	0.5		Cfl
N	32		Number of elements for the 1D model
N_s	32		Number of elements in the s direction
N_θ	32		Number of elements in the θ direction
p	2		Polynomial degree

$A_0(s, \theta) = \frac{1}{2} \left(R_0 + (R_1 - R_0) e^{-\left(\frac{s-L}{2}\right)^2} \left(e^{-\theta^2} + e^{-(\theta-2\pi)^2} \right) \right)^2$. The mild aneurysm is defined by $R_1 = 0.6$ and the severe one by $R_1 = 2$ (see **Figure 12**).

To compare the results issue from the 1D model to the 2D model, we integrate the numerical results from the 2D model over θ . The numerical results are presented in **Figure 13** and **Figure 14**. We show the behavior in time of the pressure, the speed, and the maximum angular speed at the point $\frac{L}{2}$. As expected, in the case of a mild aneurysm, since the geometry of the artery is almost cylindrical, the results from the 1D and the 2D models are almost similar (see **Figure 13**). Whenever the aneurysm is severe, the geometry is no longer almost cylindrical, at least around the aneurysm, and important differences can be observed as shown in **Figure 14**. This is mainly because the angular speed is not zero in this case and can take large values. The 2D model can in practice compute more realistic solutions than the 1D one. The same observation holds at the control point $3L/4$. After the aneurysm, even if the geometry is cylindrical since the blood

passed away a zone where the angular speed was not 0 (see **Figure 15** and **Figure 16**), they are distinguishable difference between the 1D and the 2D models which confirms the limit of the 1D model. The more the amplitude of the maximum angular speed is, the more the difference observed between the 1D and the 2D models is. Note that the 2D model is computationally more demanding than the 1D one. For example, in the case of tableTC4, it requires $32 \times 32 \times (2+1)^2 = 9216$ DDOF per variable, whereas the 1D model only needs $32 \times (2+1) = 96$ DDOF. Nevertheless, the cost remains far lower than in the 3D case, which would involve $32 \times 32 \times 32 \times (2+1)^3 = 884736$ DDOF for a similar configuration, not to mention the additional mesh adaptation required in 3D.

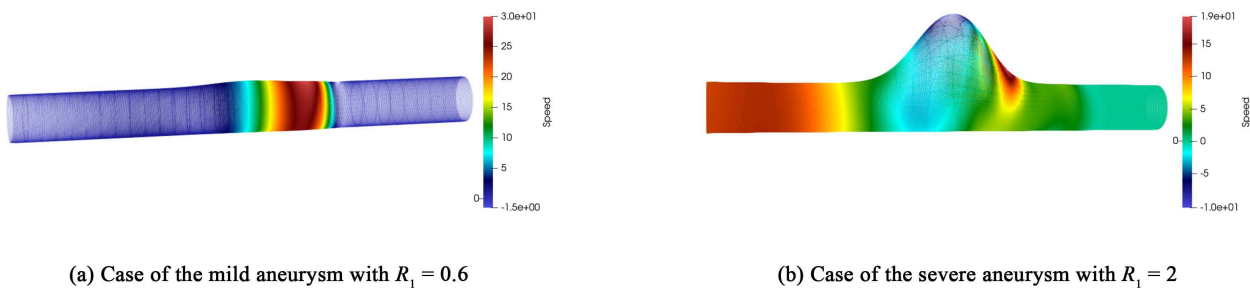


Figure 12. Initial geometry and Speed for the 2D at $t = \frac{T}{2}$.

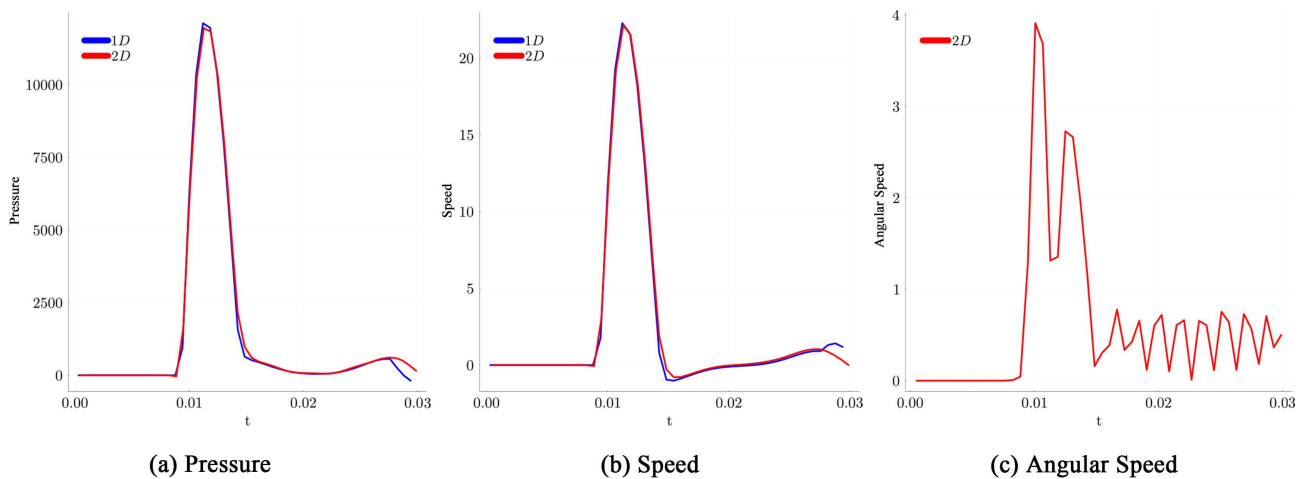


Figure 13. Pressure, axial speed and maximum angular speed for the 2D and 1D model at the point $\frac{L}{2}$ for $R_1 = 0.6$.

5. Conclusion

In conclusion, we have developed a new two-dimensional model for blood flow simulations, for which we implemented a discontinuous Galerkin method. We have determined several mathematical and numerical properties, notably establishing that the scheme we constructed is well-balanced. Furthermore, through various test cases, we demonstrated the robustness of our method. Specifically, we compared 1D models with the 2D model in the context of both severe and

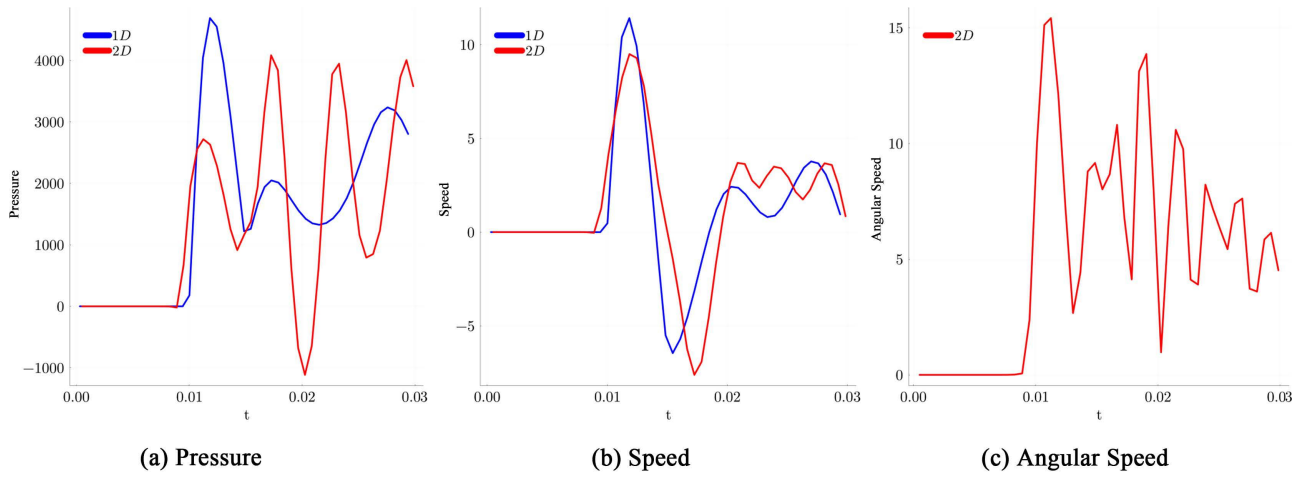


Figure 14. Pressure and Speed for the 2D and 1D model at the point $\frac{L}{2}$ for $R_1 = 2$.

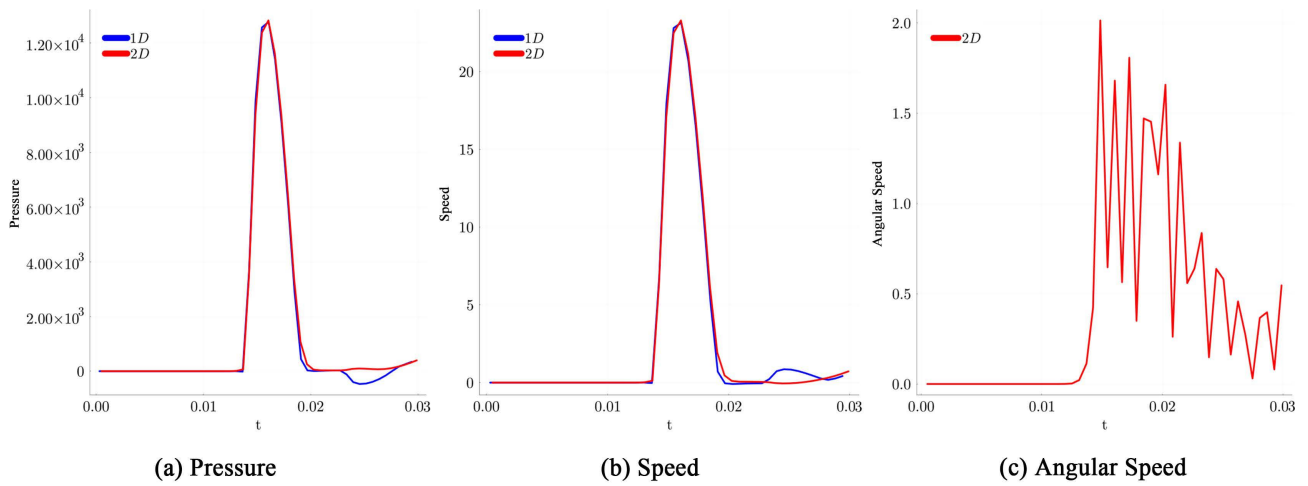


Figure 15. Pressure, axial speed and maximum angular speed for the 2D and 1D model at the point $\frac{3L}{4}$ for $R_1 = 0.6$.

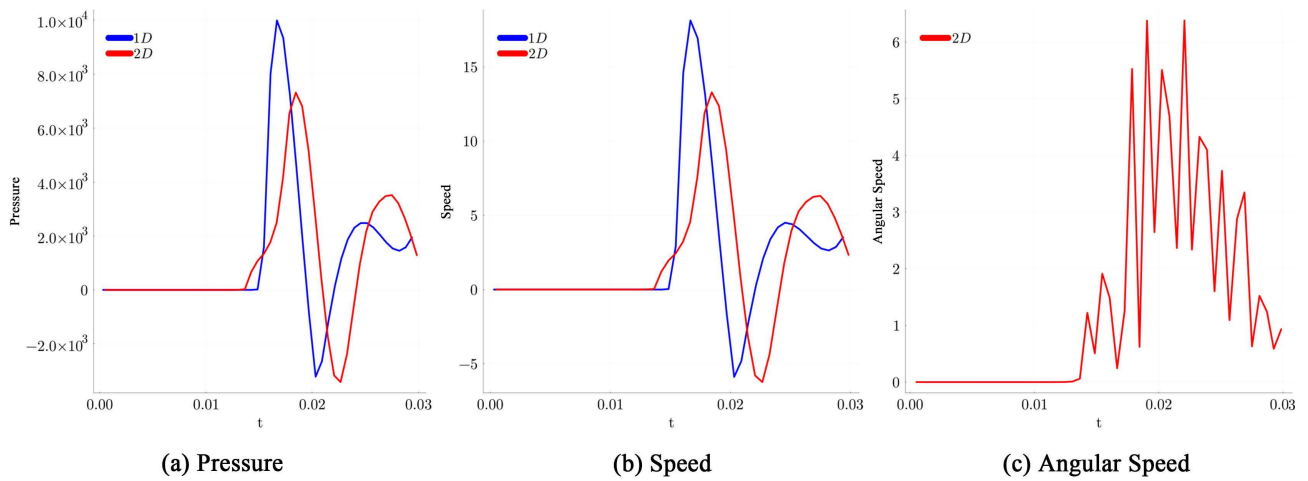


Figure 16. Pressure, axial speed and maximum angular speed for the 2D and 1D model at the point $\frac{3L}{4}$ for $R_1 = 2$.

mild aneurysms. This test case highlighted the limitations of 1D models. Beyond these achievements, the proposed model has potential clinical relevance, particularly for improving the understanding of blood flow in pathological situations such as aneurysms or stenoses. Future work will focus on validating the model against experimental or clinical data, which is essential to assess its predictive capabilities. In addition, coupling this approach with patient-specific geometries could make the model a valuable tool for surgical planning or for evaluating treatment strategies. Further research will also aim at extending the framework to more complex arterial wall models and at investigating the role of hyperelasticity in aneurysm growth and rupture.

Acknowledgements

This work has been supported by the ADEN-MED project (Adaptability to Extreme events and Natural risks -application to the Mediterranean and Djibouti), funded by the Région Sud Provence-Alpes-Côte d'Azur under the AAP MEDCLIMAT "Natural risks and food sovereignty"?

Conflicts of Interest

The authors declare no conflicts of interest regarding the publication of this paper.

References

- [1] Formaggia, L., Nobile, F. and Quarteroni, A. (2002) A One-Dimensional Model for Blood Flow: Application to Vascular Prosthesis. *Mathematical Modeling and Numerical Simulation in Continuum Mechanics. Proceedings of the International Symposium on Mathematical Modeling and Numerical Simulation in Continuum Mechanics*, Yamaguchi, 29 September-3 October 2000, 137-153. https://doi.org/10.1007/978-3-642-56288-4_10
- [2] Formaggia, L., Gerbeau, J.F., Nobile, F. and Quarteroni, A. (2001) On the Coupling of 3D and 1D Navier-Stokes Equations for Flow Problems in Compliant Vessels. *Computer Methods in Applied Mechanics and Engineering*, **191**, 561-582. [https://doi.org/10.1016/s0045-7825\(01\)00302-4](https://doi.org/10.1016/s0045-7825(01)00302-4)
- [3] Čanić, S. and Kim, E.H. (2003) Mathematical Analysis of the Quasilinear Effects in a Hyperbolic Model Blood Flow through Compliant Axi-Symmetric Vessels. *Mathematical Methods in the Applied Sciences*, **26**, 1161-1186. <https://doi.org/10.1002/mma.407>
- [4] Čanić, S. (2002) Blood Flow through Compliant Vessels after Endovascular Repair: Wall Deformations Induced by the Discontinuous Wall Properties. *Computing and Visualization in Science*, **4**, 147-155. <https://doi.org/10.1007/s007910100066>
- [5] Berntsson, F., Ghosh, A., Kozlov, V.A. and Nazarov, S.A. (2018) A One-Dimensional Model of Blood Flow through a Curvilinear Artery. *Applied Mathematical Modelling*, **63**, 633-643. <https://doi.org/10.1016/j.apm.2018.07.019>
- [6] Quarteroni, A. and Formaggia, L. (2004) Mathematical Modelling and Numerical Simulation of the Cardiovascular System. In: *Handbook of Numerical Analysis*, Elsevier, 3-127. [https://doi.org/10.1016/s1570-8659\(03\)12001-7](https://doi.org/10.1016/s1570-8659(03)12001-7)
- [7] Ventre, J. (2020) Reduced-Order Models for Blood Flow in the Large Arteries: Applications to Cardiovascular Pathologies. PhD Thesis, Sorbonne Université.

- [8] Krivovichev, G.V. (2022) Computational Analysis of One-Dimensional Models for Simulation of Blood Flow in Vascular Networks. *Journal of Computational Science*, **62**, Article ID: 101705. <https://doi.org/10.1016/j.jocs.2022.101705>
- [9] Azer, K. and Peskin, C.S. (2007) A One-Dimensional Model of Blood Flow in Arteries with Friction and Convection Based on the Womersley Velocity Profile. *Cardiovascular Engineering*, **7**, 51-73. <https://doi.org/10.1007/s10558-007-9031-y>
- [10] Nardinocchi, P., Pontrelli, G. and Teresi, L. (2005) A One-Dimensional Model for Blood Flow in Prestressed Vessels. *European Journal of Mechanics—A/Solids*, **24**, 23-33. <https://doi.org/10.1016/j.euromechsol.2004.10.002>
- [11] Huo, Y. and Kassab, G.S. (2007) A Hybrid One-Dimensional/Womersley Model of Pulsatile Blood Flow in the Entire Coronary Arterial Tree. *American Journal of Physiology—Heart and Circulatory Physiology*, **292**, H2623-H2633. <https://doi.org/10.1152/ajpheart.00987.2006>
- [12] Fung, Y.-C. (2013) *Biomechanics: Mechanical Properties of Living Tissues*. Springer Science & Business Media.
- [13] Ersoy, M. (2015) Dimension Reduction for Incompressible Pipe and Open Channel Flow Including Friction. *Conference Applications of Mathematics 2015, in Honor of the 90th Birthday of Ivo Babuška and 85th Birthday of Milan Práger and Emil Vitásek*, Prague, November 2015, 17-33.
- [14] Ersoy, M., Lakkis, O. and Townsend, P. (2020) A Saint-Venant Model for Overland Flows with Precipitation and Recharge. *Mathematical and Computational Applications*, **26**, Article No. 1. <https://doi.org/10.3390/mca26010001>
- [15] Gerbeau, J. and Perthame, B. (2001) Derivation of Viscous Saint-Venant System for Laminar Shallow Water; Numerical Validation. *Discrete & Continuous Dynamical Systems—B*, **1**, 89-102. <https://doi.org/10.3934/dcdsb.2001.1.89>
- [16] Ersoy, M. (2016) Dimension Reduction for Compressible Pipe Flows Including Friction. *Asymptotic Analysis*, **98**, 237-255. <https://doi.org/10.3233/asy-161367>
- [17] Grinberg, L., Cheever, E., Anor, T., Madsen, J.R. and Karniadakis, G.E. (2010) Modeling Blood Flow Circulation in Intracranial Arterial Networks: A Comparative 3D/1D Simulation Study. *Annals of Biomedical Engineering*, **39**, 297-309. <https://doi.org/10.1007/s10439-010-0132-1>
- [18] Cockburn, B. (2003) Discontinuous Galerkin Methods. *ZAMM—Journal of Applied Mathematics and Mechanics*, **83**, 731-754. <https://doi.org/10.1002/zamm.200310088>
- [19] Debyaoui, M.A. and Ersoy, M. (2021) A Generalised Serre-Green-Naghdi Equations for Variable Rectangular Open Channel Hydraulics and Its Finite Volume Approximation. In: Muñoz-Ruiz, M.L., et al., Eds., *Recent Advances in Numerical Methods for Hyperbolic PDE Systems: NumHyp 2019*, Springer International Publishing, 251-268. https://doi.org/10.1007/978-3-030-72850-2_11
- [20] Poussel, C. (2024) Dynamics of Free-Surface and Groundwater Flows in Sandy Beaches. PhD Thesis, Université de Toulon.
- [21] Poussel, C., Ersoy, M., Golay, F. and Mannes, Y. (2023) Runge-Kutta Discontinuous Galerkin Method Applied to Shallow Water Equations. In: *Topical Problems of Fluid Mechanics 2023*, Institute of Thermomechanics of the Czech Academy of Sciences, 152-159.
- [22] Clément, J.-B. (2021) Numerical Simulation of Flows in Unsaturated Porous Media by an Adaptive Discontinuous Galerkin Method: Application to Sandy Beaches. PhD Thesis, Université de Toulon.
- [23] Butcher, J.C. (1996) A History of Runge-Kutta Methods. *Applied Numerical Mathe-*

-
- matics*, **20**, 247-260. [https://doi.org/10.1016/0168-9274\(95\)00108-5](https://doi.org/10.1016/0168-9274(95)00108-5)
- [24] Cockburn, B. and Shu, C. (2001) Runge-Kutta Discontinuous Galerkin Methods for Convection-Dominated Problems. *Journal of Scientific Computing*, **16**, 173-261. <https://doi.org/10.1023/a:1012873910884>
- [25] Gottlieb, S., Ketcheson, D.I. and Shu, C. (2008) High Order Strong Stability Preserving Time Discretizations. *Journal of Scientific Computing*, **38**, 251-289. <https://doi.org/10.1007/s10915-008-9239-z>
- [26] Mannes, Y., Ersoy, M., Eker, Ö.F. and Ajroud, A. (2025) On the Derivation of a New One-Dimensional Model for Blood Flows and Its Numerical Approximation. *Journal of Applied Mathematics and Physics*, **13**, 3479-3514. <https://doi.org/10.4236/jamp.2025.1310198>
- [27] Merritt, W.C., Berns, H.F., Ducruet, A.F. and Becker, T.A. (2021) Definitions of Intracranial Aneurysm Size and Morphology: A Call for Standardization. *Surgical Neurology International*, **12**, Article No. 506. https://doi.org/10.25259/sni_576_2021